AMERICAN SOCIETY FOR MICROBIOLOGY | Infection and Immunity®

FUNGAL AND PARASITIC INFECTIONS

Hookworm-Derived Metabolites Suppress Pathology in a Mouse Model of Colitis and Inhibit Secretion of Key Inflammatory Cytokines in Primary Human Leukocytes

Phurpa Wangchuk,[a] Catherine Shepherd,[a] Constantin Constantinoiu,[b] Rachael Y. M. Ryan,[a] Konstantinos A. Kouremenos,[c] Luke Becker,[a] Linda Jones,[a] Geraldine Buitrago,[a] Paul Giacomin,[a] David Wilson,[a] Norelle Daly,[a] Malcolm J. McConville,[c] John J. Miles,[a] Alex Loukas[a]

[a]Centre for Biodiscovery and Molecular Development of Therapeutics, Australian Institute of Tropical Health and Medicine, James Cook University, Cairns, Australia
[b]College of Public Health, Medical and Veterinary Sciences, Centre for Biosecurity in Tropical Infectious Diseases, James Cook University, Townsville, Australia
[c]Metabolomics Australia, Bio21 Molecular Science and Biotechnology Institute, University of Melbourne, Parkville, Australia

ABSTRACT Iatrogenic hookworm therapy shows promise for treating disorders that result from a dysregulated immune system, including inflammatory bowel disease (IBD). Using a murine model of trinitrobenzenesulfonic acid-induced colitis and human peripheral blood mononuclear cells, we demonstrated that low-molecular-weight metabolites derived from both somatic extracts (LMWM-SE) and excretory-secretory products (LMWM-ESP) of the hookworm, *Ancylostoma caninum*, display anti-inflammatory properties. Administration to mice of LMWM-ESP as well as sequentially extracted fractions of LMWM-SE using both methanol (SE-MeOH) and hexane-dichloromethane-acetonitrile (SE-HDA) resulted in significant protection against T cell-mediated immunopathology, clinical signs of colitis, and impaired histological colon architecture. To assess bioactivity in human cells, we stimulated primary human leukocytes with lipopolysaccharide in the presence of hookworm extracts and showed that SE-HDA suppressed *ex vivo* production of inflammatory cytokines. Gas chromatography-mass spectrometry (MS) and liquid chromatography-MS analyses revealed the presence of 46 polar metabolites, 22 fatty acids, and five short-chain fatty acids (SCFAs) in the LMWM-SE fraction and 29 polar metabolites, 13 fatty acids, and six SCFAs in the LMWM-ESP fraction. Several of these small metabolites, notably the SCFAs, have been previously reported to have anti-inflammatory properties in various disease settings, including IBD. This is the first report showing that hookworms secrete small molecules with both *ex vivo* and *in vivo* anti-inflammatory bioactivity, and this warrants further exploration as a novel approach to the development of anti-inflammatory drugs inspired by coevolution of gut-dwelling hookworms with their vertebrate hosts.

KEYWORDS *Ancylostoma caninum*, excretory-secretory product, hookworm, metabolomics, small molecule, helminths

Inflammatory bowel disease (IBD) is associated with chronic inflammation of the digestive tract and primarily includes ulcerative colitis (UC) and Crohn's disease (CD). The etiology of IBD is not well established, but the disease is usually characterized by inflammation, loss of appetite and weight, chronic diarrhea, bloody stools, fever, rectal bleeding, abdominal pain, fatigue, and anemia (1–3). IBD has been linked to many extraintestinal manifestations (4) and implicated with mental health problems (5). Current treatments for IBD include 5-aminosalicylates, glucocorticosteroids, immunomodulators and biologics, and proctocolectomy as a last resort when drug treatment fails. Many of these drugs are often associated with side effects and various postoperative complications (6, 7). Frontline biologics such as treatment with anti-tumor necro-

Citation Wangchuk P, Shepherd C, Constantinoiu C, Ryan RYM, Kouremenos KA, Becker L, Jones L, Buitrago G, Giacomin P, Wilson D, Daly N, McConville MJ, Miles JJ, Loukas A. 2019. Hookworm-derived metabolites suppress pathology in a mouse model of colitis and inhibit secretion of key inflammatory cytokines in primary human leukocytes. Infect Immun 87:e00851-18. https://doi.org/10.1128/IAI.00851-18.

Editor De'Broski R. Herbert, University of Pennsylvania

Address correspondence to Phurpa Wangchuk, phurpa.wangchuk@jcu.edu.au, or Alex Loukas, alex.loukas@jcu.edu.au.

P.W. and C.S. contributed equally to this article.

Received 28 November 2018
Accepted 15 January 2019
Accepted manuscript posted online 22 January 2019
Published 25 March 2019

sis factor (anti-TNF) monoclonal antibodies are efficacious in only some patients, and treatment does not result in long-term cure (8). Failure of these frontline treatments is associated with elevated risk of colon cancer and can result in the need for surgical removal of the colon (partial or full). Therefore, there is an urgent need for new and effective anti-inflammatory drugs to treat IBD.

Guided by millennia of host-parasite coevolution, we (9–13) and others (14–16) have demonstrated the therapeutic properties of experimental hookworm infection to treat gastrointestinal (GI) inflammatory diseases. Hookworms resident in the human GI tract induce tolerogenic dendritic cells and regulatory T cells which produce suppressor cytokines that keep inflammatory T cells and their effector molecules in check (17, 18). While iatrogenic hookworm therapy shows promise for treating numerous inflammatory diseases in humans, it presents many challenges, including apprehension by the patient to readily accept such a radical intervention, safety concerns, and regulatory hurdles. In order to circumvent these limitations, we have investigated whether the immunomodulatory properties of hookworms are due to specific metabolites in the parasite's somatic tissue or excretory/secretory products (ESP). Administration of hookworm ESP to mice protected against inflammation and weight loss in two different mouse models of chemically induced colitis: the T cell-dependent trinitrobenzene sulfonic acid (TNBS) model (19) and the T cell-independent dextran sulfate sodium (DSS) model (20). We previously characterized the protein constituents (>10 kDa) of hookworm ESP (21) and identified a protein, anti-inflammatory protein 2 from *Ancylostoma caninum* (*Ac*-AIP-2), which in recombinant form displayed immunomodulatory properties in a mouse model of asthma that was dependent on regulatory T cells and tolerogenic dendritic cells (22). A related protein termed *Ac*-AIP-1 also displayed anticolitic effects in mice by inducing accumulation of regulatory T cells in the mucosa and production of suppressor cytokines, including interleukin 10 (IL-10) and transforming growth factor β (TGF-β) (23).

While the protein constituents of hookworm ESP are well characterized in terms of their ontologies and anti-inflammatory properties, the efficacy of nonproteogenic, low-molecular-weight metabolites (LMWM) in hookworm ESP remain unexplored (24). Secreted LMWM may be the products of overflow metabolites or have other roles, such as in signaling. For example, other nematodes, namely, the parasitic *Ascaris lumbricoides* and free-living *Caenorhabditis elegans*, produce biologically active LMWM, including ascarosides and short-chain fatty acids (SCFAs), that have diverse biological properties (25). We therefore hypothesized that parasitic nematodes such as hookworms produce LMWM, some of which might have immunoregulatory properties and therefore present as potential anti-inflammatory drug candidates. Using the TNBS model of colitis, we demonstrated that selected crude hookworm LMWM extracts sourced from both ESP and somatic extracts (SE) afford significant protection against inducible acute colitis in mice and suppress *ex vivo* inflammatory cytokine production from human peripheral blood mononuclear cells (PBMC). Metabolomics analyses of the LMWM-ESP and LMWM-SE of the dog hookworm *Ancylostoma caninum* using gas chromatography-mass spectrometry (GC-MS) and liquid chromatography-mass spectrometry (LC-MS) highlighted potential anti-inflammatory candidates.

RESULTS

We analyzed the anti-inflammatory role of LMWM-ESP and LMWM-SE of adult *A. caninum*, using the TNBS model of colitis. These fractions were collected separately and analyzed independently for two main reasons: (i) ESP were initially collected for the purpose of protein analysis (not LMWM), and at the time, we only had access to snap-frozen adult hookworms for LMWM extraction; (ii) later, we obtained access to a sufficient number of live hookworms to collect ESP for this study. The findings of the studies are presented below in four parts: (i) *in vivo* anti-inflammatory activities of LMWM-SE in TNBS-colitis, (ii) *in vivo* anti-inflammatory activities of hookworm LMWM-ESP in TNBS-colitis, (iii) *ex vivo* anti-inflammatory activities of hookworm LMWM-ESP and LMWM-SE on lipopolysaccharide (LPS)-activated human peripheral blood mono-

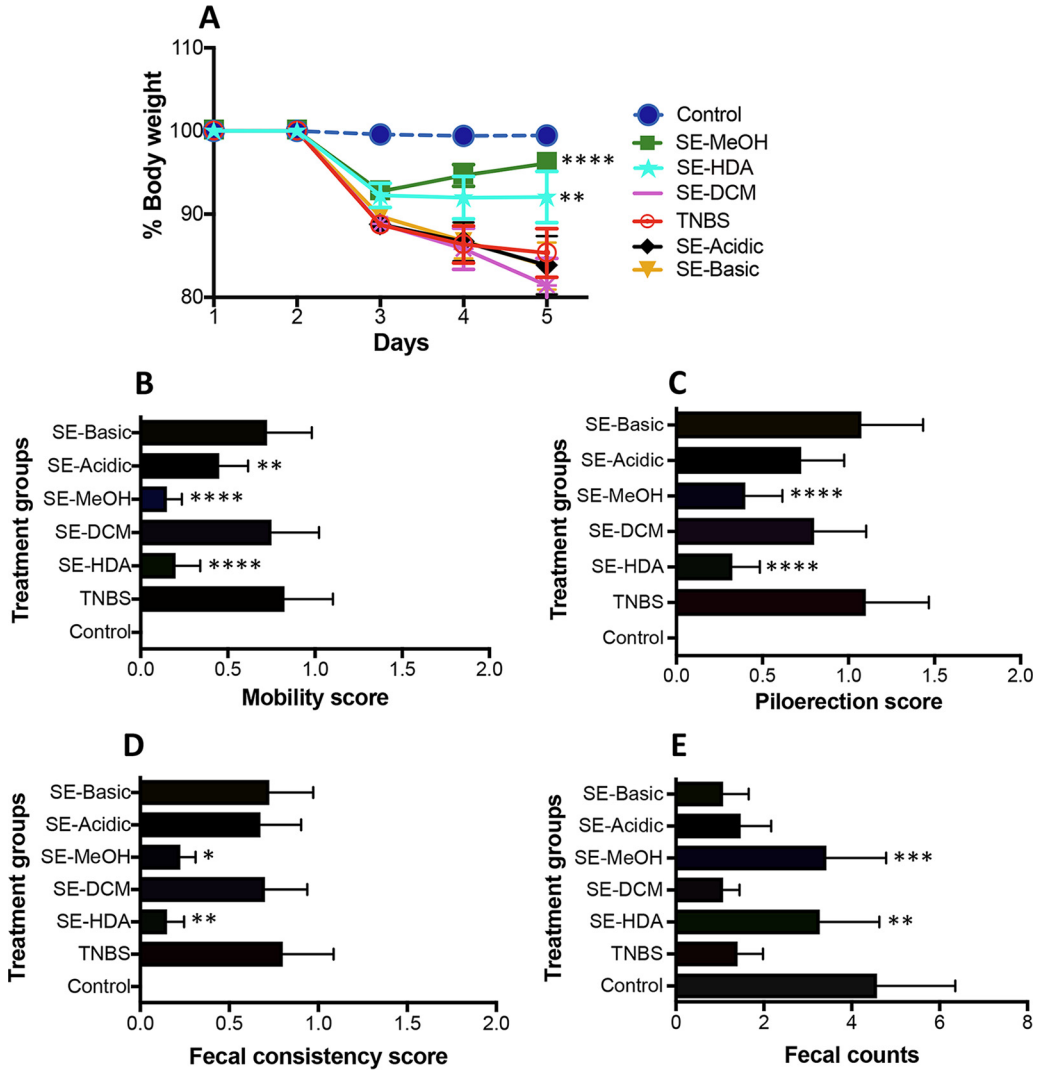

FIG 1 Protective effects of intraperitoneal administration of LMWM-SE of *A. caninum* against different clinical symptoms of TNBS-induced colitis in mice ($n = 10$). (A) Percent change in body weight; (B) mobility score; (C) piloerection score; (D) fecal consistency score; (E) fecal pellet counts. Statistical analyses were performed using GraphPad Prism 7 (2-way ANOVA). *, $P < 0.05$; **, $P < 0.01$; ***, $P < 0.001$; ****, $P < 0.0001$.

nuclear cells, and (iv) metabolome profiles of both hookworm LMWM-ESP and LMWM-SE. The metabolomics studies included targeted identification of polar metabolites and fatty acids.

LMWM-SE of hookworms protect mice against TNBS-induced colitis. For acquiring LMWM-SE, we used a natural products extraction protocol by sequentially extracting the ground powder with different solvents, including mixed solvents of hexane-dichloromethane-acetronitrile (1:1:1 vol/vol; HDA), followed by dichloromethane (DCM), methanol (MeOH), acidified aqueous (Acidic), and alkaline aqueous (Basic) solutions. This extraction yielded five LMWM-SE fractions termed SE-HDA, SE-DCM, SE-MeOH, SE-Acidic, and SE-Basic, all of which were tested for their anti-inflammatory activities using a modified murine TNBS-colitis experimental design as previously described (26). All five extracts were administered intraperitoneally (i.p.; 50 μg/mouse) prior to intrarectal (i.r.) injection of TNBS. Mice were monitored daily for 3 days for progression of clinical symptoms of colitis. Of the five somatic tissue extracts tested, SE-HDA and SE-MeOH significantly protected mice against TNBS-induced clinical symptoms of colitis, including body weight loss, lethargy (mobility), piloerection, and fecal inconsistency (Fig. 1).

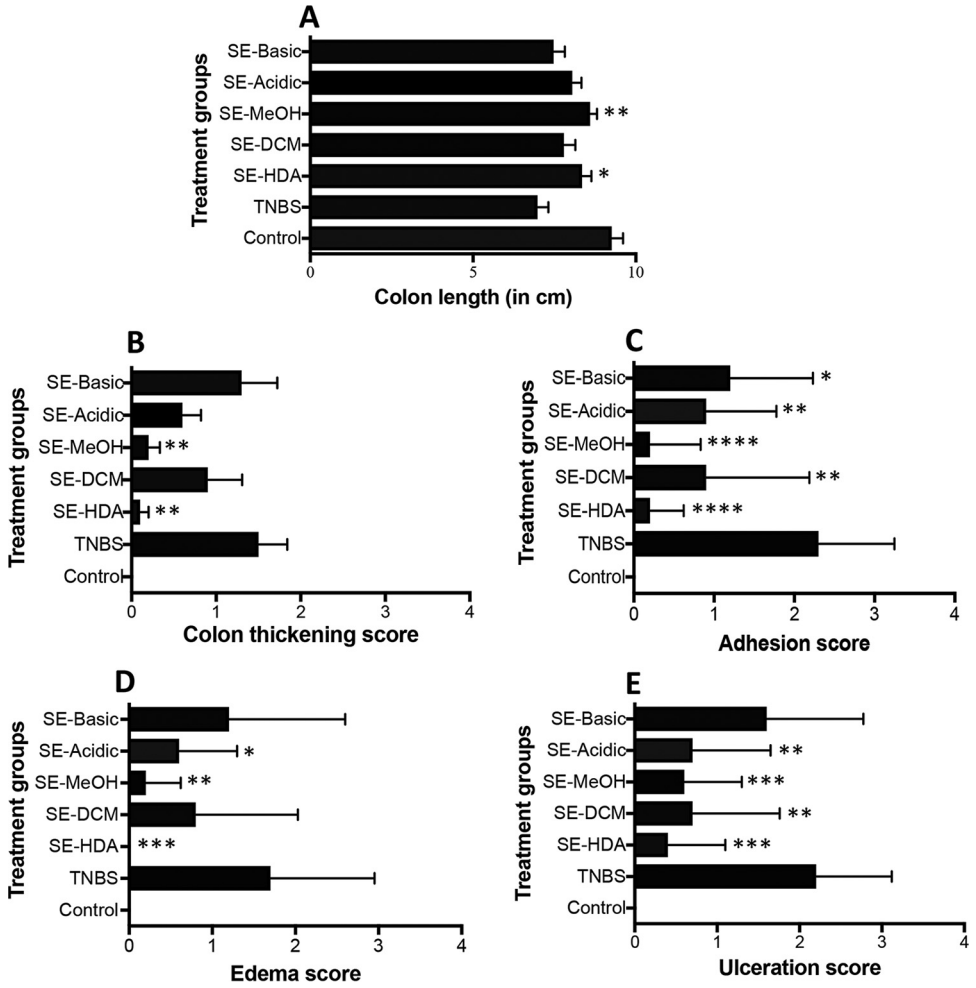

FIG 2 Macroscopic pathology scores of mice treated with different LMWM-SE of *A. caninum* ($n = 10$). (A) Colon length; (B) colon wall thickening score; (C) adhesion score; (D) edema score; (E) ulceration score. Statistical analyses were performed using GraphPad Prism 7.

Upon euthanasia, mouse colons were scored for pathological progression of colitis and then colon tissues were processed for histopathology and cytokine profiles. In congruence with the clinical scores, colons of mice treated with SE-HDA and SE-MeOH extracts showed significantly less colonic pathology than those of untreated mice, as indicated by longer colon lengths (Fig. 2A), reduced colon thickening (Fig. 2B), fewer adhesions (Fig. 2C), less edema (Fig. 2D), and less ulceration (Fig. 2E).

The SE-HDA and SE-MeOH treated animals also showed well-preserved colon architecture in comparison to that of the TNBS control group (Fig. 3). Naive mice (healthy control group) showed normal colon tissue architecture with healthy crypts and goblet cell numbers and normal lamina propria and mucosal integrity.

Mice that were administered TNBS only (not treated with extracts) developed colitis and exhibited severe thickening of the lamina propria and colon wall musculature, edema, mucosal erosion, and destruction of goblet cells. Increased numbers of leukocytes and polymorphonuclear cell infiltrates were clearly evident in the lamina propria and intraepithelial compartments of colons from untreated mice administered TNBS. Treatment with SE-HDA and SE-MeOH hookworm extracts significantly protected mice against TNBS-induced histological damage. Treated mice had well-formed crypts and large numbers of goblet cells and displayed generally healthy mucosal integrity that was comparable to that of naive mice that did not receive TNBS. The other three hookworm LMWM-SE, including SE-DCM, SE-Acidic, and SE-Basic did not protect mice

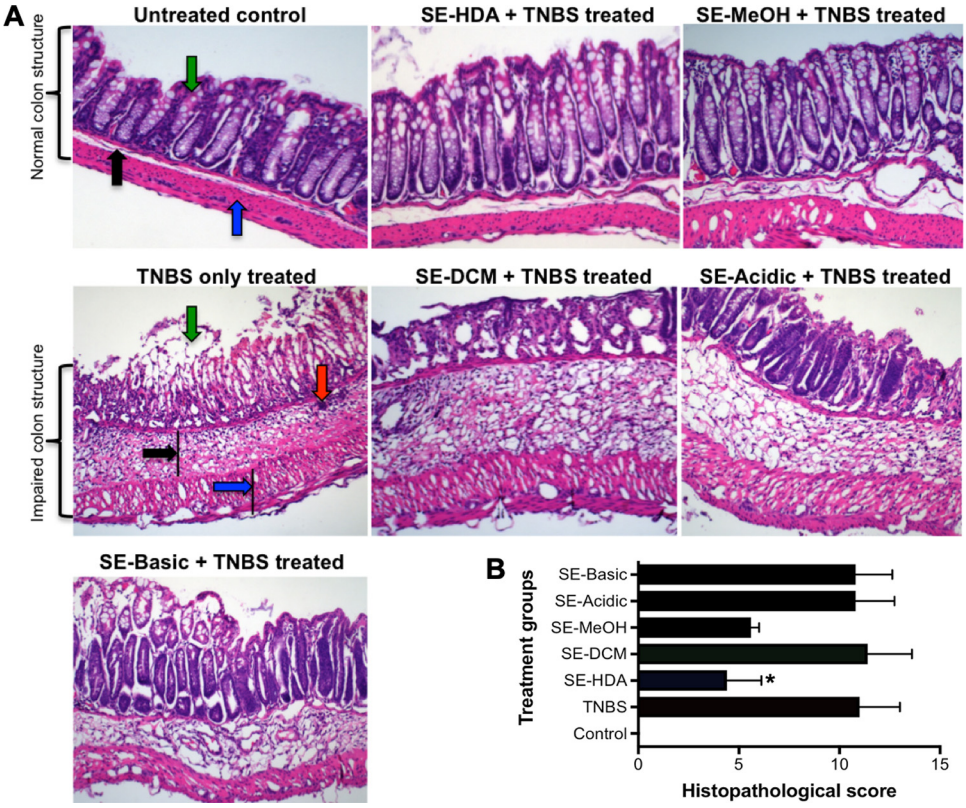

FIG 3 Administration of SE-HDA and SE-MeOH protected mice against TNBS-induced colonic inflammation. (A) Representative histological photomicrographs of hematoxylin and eosin (H&E)-stained paraffin sections (×200) of distal colon tissues of an untreated mouse with normal goblet cells (green arrow), lamina propria (black arrow), and colon wall (blue arrow); TNBS control mouse colon showed erosion of goblets cells (green arrow), thickening of lamina propria (black arrow), cell infiltration (red arrow), and colon wall thickening (blue arrow). Mice treated with SE-HDA/TNBS and SE-MeOH/TNBS showed less pathology than untreated mice that received TNBS. Mice treated with SE-DCM/TNBS, SE-Acidic/TNBS, and SE-Basic/TNBS were not protected against colitic immunopathology. (B) Scoring of histological outcomes of all treatment groups for pathological changes. Statistical analyses were performed using Graphpad Prism 7 (one-way ANOVA).

against histopathological damage induced by TNBS. Scoring of histological sections for overall colon pathology showed that mice treated with SE-HDA had significantly reduced histopathology, whereas the SE-MeOH-treated group demonstrated a nonsignificant trend toward reduced histopathology, compared with TNBS control mice. Colon tissues were cultured to collect supernatants for assessment of colonic cytokine secretion. Colon culture supernatants from SE-HDA- and SE-MeOH-treated mice were analyzed for a panel of nine cytokines, including IL-1β, IL-4, IL-5, IL-6, IL-10, IL-13, IL-12p70, and gamma interferon (IFN-γ). No signficaint differences were detected, and only IFN-γ, IL-17A, IL-1β, and IL-13 showed statistically nonsignificant downward trends compared to untreated mice that received TNBS (see Fig. S1 in the supplemental material).

LMWM-ESP protects mice against TNBS colitis. In line with the anti-inflammatory effects of LMWM-SE, mice treated with LMWM-ESP were also protected against TNBS-induced colitis. Clinically, we detected statistically significant protection against weight loss, colon shortening, and clinical parameters of colitis (including piloerection, mobility, and fecal consistency) compared to those of untreated mice that received TNBS (Fig. 4).

Macroscopically, mice treated with LMWM-ESP showed significant reductions in disease progression/pathology scores compared to those of untreated mice that were administered TNBS (Fig. 5).

Colon tissue was stained with hematoxylin and eosin (H&E), and blind scoring (maximum total of 16 points) for ulceration, infiltration of the muscularis mucosa,

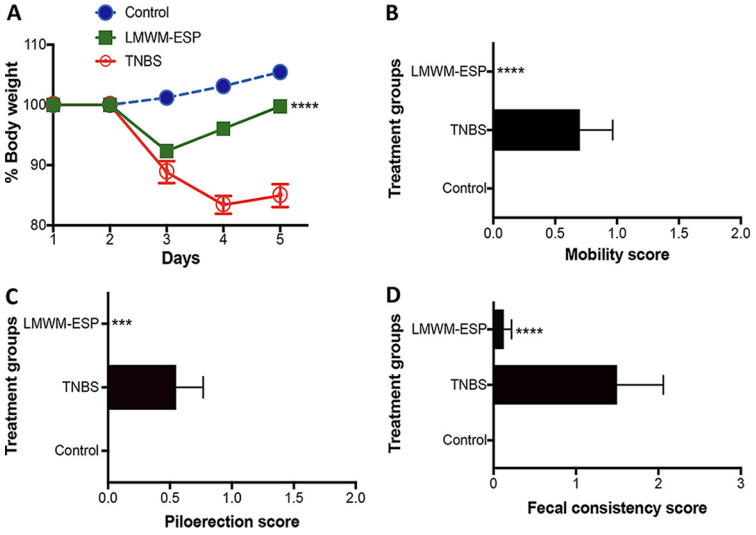

FIG 4 Protective effects of *A. caninum* LMWM-ESP in the TNBS model of murine colitis. (A) Percent change in body weight; (B) mobility score; (C) piloerection score; (D) fecal consistency score. All results are the aggregation of those from at least two independent experiments. Treatment groups received 50 μg of material per mouse via i.p. injection (n =10). Statistical analyses were performed using GraphPad Prism 7 (2-way ANOVA).

overall integrity of the epithelium, and the presence of lymphoid follicles was carried out. Mice treated with 50 μg of LMWM-ESP showed significantly less immunopathology than untreated mice that received TNBS and had lower histological scores (Fig. 6).

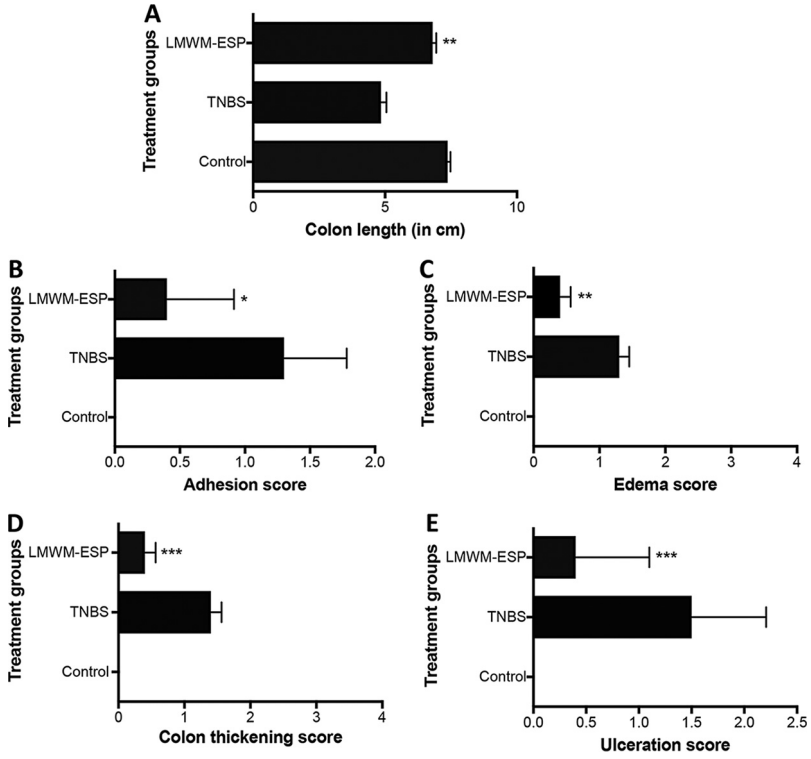

FIG 5 Macroscopic pathology scores of mice treated via i.p. injection with 50 μg of LMWM-ESP prior to administration of TNBS. (A) Colon length; (B) colon adhesion score; (C) colon edema score; (D) colon thickening score; (E) colon ulceration score. All results are the aggregation of those from at least two independent experiments (n =10). Statistical analyses were performed using GraphPad Prism 7 (one-way ANOVA).

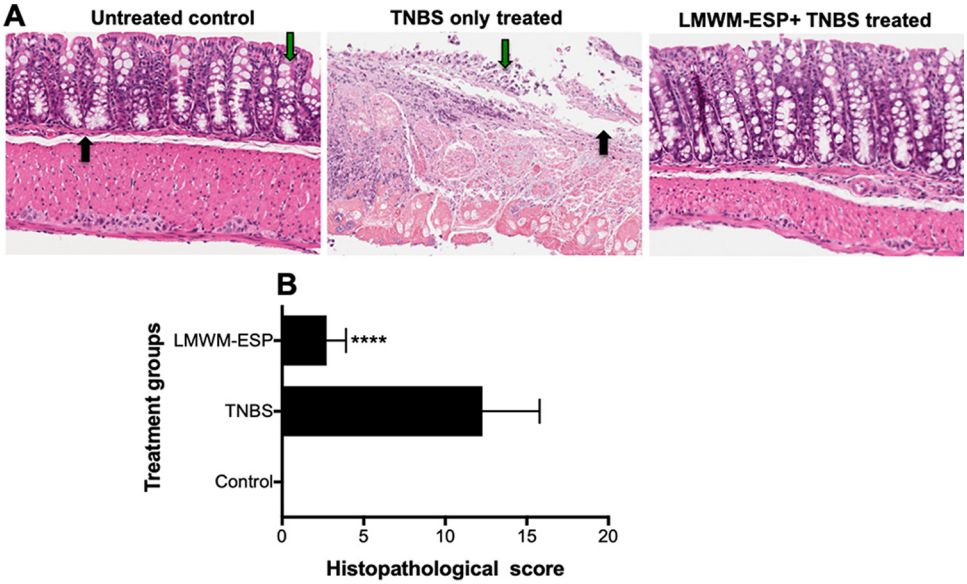

FIG 6 Representative histological architecture of the colons of mice that received i.p. injection of 50 μg of *A. caninum* LMWM-ESP. Longitudinal sections of mouse colon were stained with hematoxylin & eosin. (A) Naive or untreated control colon displayed healthy crypts and goblet cells (green arrow) and lamina propria (black arrow); for TNBS-only treated colon, note the destruction of the mucosal layer, disappearance of goblet cells (green arrow), and thickening of lamina propria (black arrow); for the colon of a mouse treated with LMWM-ESP prior to administration of TNBS, note the maintenance of mucosal layers and relatively little immune infiltration of the tissue. (B) Aggregate blinded scoring of histopathology sections, where a score of 0 is completely normal tissue and 16 means complete destruction of tissue architecture. Statistical analyses were performed using GraphPad Prism 7 (one-way ANOVA).

Following similar protocols as described for LMWM-SE, we assessed the colon cultures from LMWM-ESP-treated mice for a number of cytokines, including IL-1β, IL-4, IL-5, IL-6, IL-13, TNF-α, TGF-β, and IFN-γ. Three key inflammatory cytokines that drive drive pathology in human ulcerative colitis—TNF-α, IL-1β, and IL-13—were significantly reduced in mice treated with LMWM-ESP compared to the levels in untreated mice that received TNBS (Fig. 7).

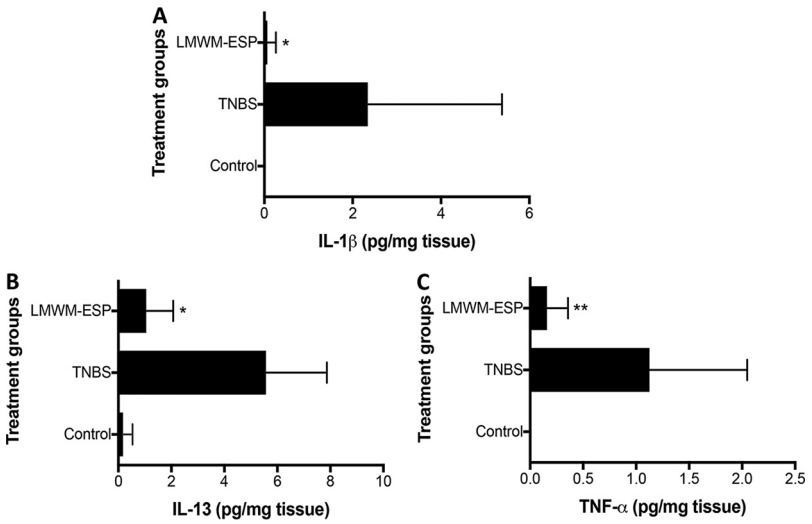

FIG 7 Changes in colon cytokine levels induced by treatment of mice with 50 μg of LMWM-ESP via i.p. injection. (A) IL-1β; (B) IL-13; (C) TNF-α. Cytokines were measured from colonic tissue cultured for 24 h in complete media. The LMWM-ESP-treated mice had significantly lower inflammatory cytokine levels than did TNBS control groups. All results are the aggregation of those from at least two independent experiments (n = 10). All cytokine results presented are normalized to tissue weight to allow for comparison across experimental groups. Statistical analyses were performed using GraphPad Prism 7 (one-way ANOVA).

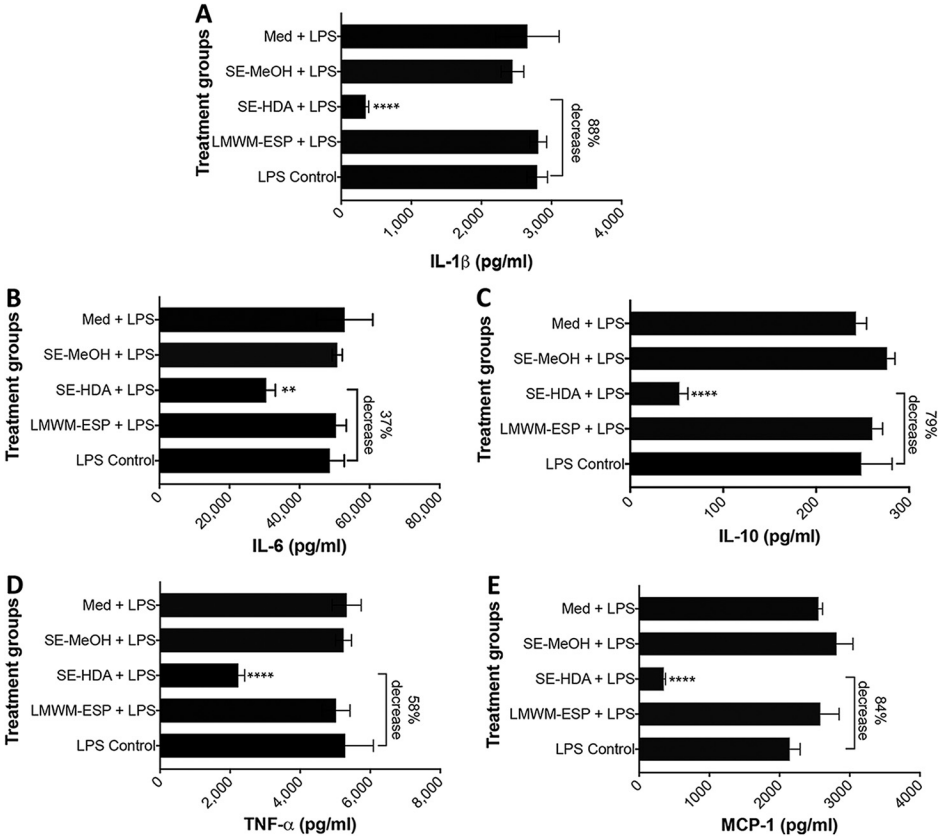

FIG 8 Coculture of human PBMC with LMWM-ESP, SE-MeOH, and SE-HDA at a final concentration of 20 μg/ml prior to stimulation with LPS resulted in significant supression of cytokines that are important in IBD. (A) IL-1β; (B) IL-6; (C) IL-10; (D) TNF-α; (E) MCP-1. Statistical analyses were performed using GraphPad Prism 7 (one-way ANOVA).

Other cytokines showed nonsignificant trends in reduction compared to the TNBS-only group.

***Ex vivo* anti-inflammatory activity of hookworm extracts on human peripheral blood mononuclear cells.** Since LMWM-SE (SE-HDA and SE-MeOH) and LMWM-ESP protected mice against TNBS-colitis, we further assessed these extracts for anti-inflammatory properties on human PBMC stimulated *ex vivo* with lipopolysaccharide (LPS) to promote cytokine production by myeloid cells or phorbol 12-myristate 13-acetate–ionomycin (PMA) to promote T cell activation and cytokine production. We first tested the samples at a single concentration (20 μg/ml), and the most active extract was then submitted to a dose-response curve with a higher number of blood donors. Of three extracts tested, only SE-HDA induced significant reduction in both T cell and myeloid cell cytokine secretion. T cell cytokine production was moderately reduced by SE-HDA treatment, which resulted in a 14% reduction in IL-2 ($P < 0.001$), a 34% reduction in IL-6 ($P < 0.05$), a 33% reduction in TNF-α ($P < 0.05$), and a 59% reduction in monocyte chemoattractant protein 1 (MCP-1) ($P < 0.001$) (Fig. S2). We observed a more potent effect of SE-HDA on suppression of myeloid cells stimualted with LPS, incuding an 88% reduction in IL-1β ($P < 0.0001$), a 37% reduction in IL-6 ($P < 0.001$), a 79% reduction in IL-10 ($P < 0.0001$), a 58% reduction in TNF-α ($P < 0.0001$), and an 84% reduction in MCP-1 ($P < 0.0001$) (Fig. 8). We did not detect reduced levels of any human cytokine in the presence of LMWM-ESP.

A dose-response analysis of the most active extract, SE-HDA, at final concentrations of 2, 10, 20, and 50 μg/ml showed that this extract significantly reduced the production of TNF-α, IL-1β, IL-6, and MCP-1 by LPS-activated PBMC in a dose-dependent manner (Fig. 9A to D). The greatest suppression was observed for MCP-1, for which exposure to

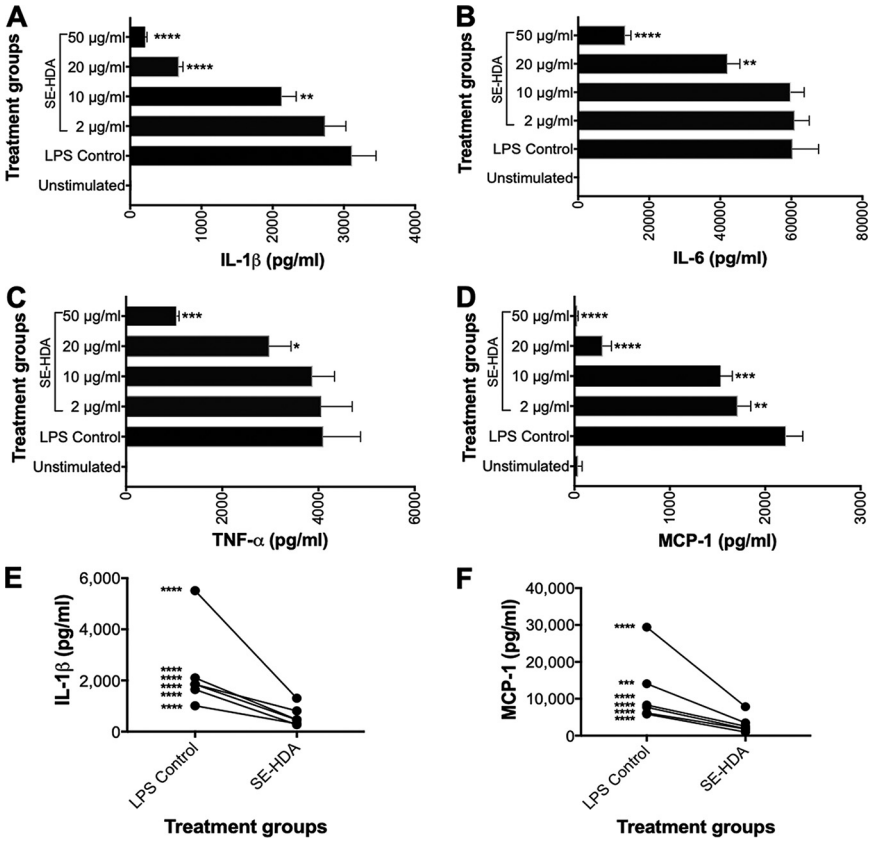

FIG 9 Dose-response effect of inflammatory cytokine and chemokine secretion by human PBMC in the presence of different concentrations of SE-HDA. Coculture with SE-HDA prior to stimulation with LPS resulted in significant suppression of the proinflammatory cytokines IL-1β (A), IL-6 (B), TNF-α (C), and MCP-1 (D). A multidonor analysis showed that SE-HDA induced significant suppression of IL-1β (E) and MCP-1 (F) in all donors. Statistical analyses were performed using GraphPad Prism 7 (one-way ANOVA).

SE-HDA concentrations as low as 2 μg/ml resulted in significantly reduced chemokine secretion. At an SE-HDA extract concentration of 50 μg/ml, LPS-stimulated MCP-1 levels were the same as those of unstimulated PBMCs. Analysis of six genetically unrelated individuals showed that SE-HDA suppression of LPS-activated PBMC was consistent across donors, with significant reductions in IL-1β, IL-6, TNF-α, and MCP-1 in all donors tested. A paired analysis of suppression in IL-1β and MCP-1 is shown in Fig. 9E and F.

Metabolomics analyses of LMWM-SE and LMWM-ESP of adult *A. caninum* reveals small molecules with known anti-inflammatory properties. To gain a global insight of metabolites present in *A. caninum*, we fractionated LMWM-SE and LMWM-ESP to obtain a biphasic partition of the solutions: upper aqueous phase (methanol-water) and lower organic phase (chloroform). Both fractions were analyzed by GC-MS after methoximation and trimethylsilyl derivitization or by LC-MS in a targeted manner. These two initial crude extracts were used to create four data sets, including (i) polar metabolome of somatic tissue extracts, (ii) nonpolar metabolome of somatic tissue extracts, (iii) polar metabolome of ESP, and (iv) nonpolar metabolome of ESP.

GC-MS-based targeted identification of polar metabolomes of adult *A. caninum* somatic tissue extract and ESP. From the LMWM-SE, we identified 46 polar small metabolites (Table S1), including amino acids, sugars, sugar phosphates, organic acids, glycerides, carbamides, and oligosaccharides. The 10 most abundant polar metabolites present in the LMWM-SE were glycine, valine, proline, glutamate (detected primarily as pyroglutamic acid in GC-MS analysis), isoleucine, tryptophan, talose, glucose, lysine, and γ-aminobutyric acid (GABA). From the LMWM-ESP, we identified 29 polar metabolites by GC-MS (Table S1), with the top 10 most abundant metabolites being pyro-

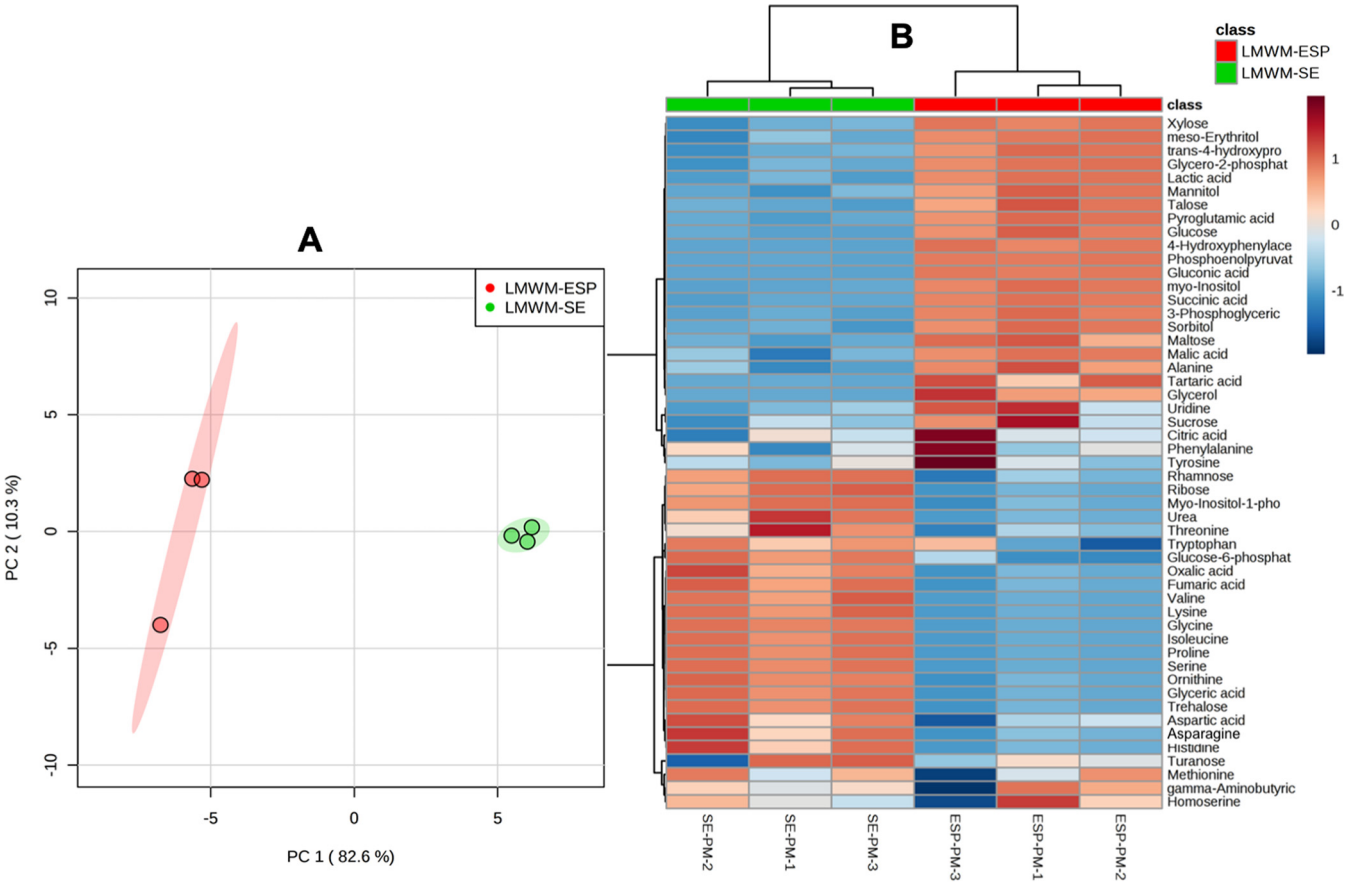

FIG 10 Multivariate analysis of the sample groups containing polar metabolites of *A. caninum*. (A) PCA score plot showing clear separation of two groups, LMWM-SE and LMWM-ESP. (B) Heat map showing unsupervised hierarchical clustering of polar metabolites present in LMWM-SE (SE-PM, somatic extract polar metabolites) and the LMWM-ESP (ESP-PM, excretory-secretory products polar metabolites) ($n = 3$ biological replicates; distance measured using Euclidean algorithm and clustering using ward.D algorithm). Data were analyzed by MetaboAnalyst 4 (samples normalized by median, log transformation, and autoscaling).

glutamic acid, trans-4-hydroxyproline, lactic acid, succinic acid, talose, glucose, alanine, maltose, *myo*-inositol, and mannitol. While 22 polar metabolites were unique to the LMWM-SE, only 5 polar metabolites were unique to the LMWM-ESP (Table S1). Twenty-four metabolites were common to both extracts.

We conducted a multivariate chemometric analysis of LMWM-SE and the LMWM-ESP, which displayed good separation in a principal-component analysis (Fig. 10A). This indicated that these two groups contained significantly different arrays of metabolites (with differences in abundance). Cluster analysis of LMWM-SE and the LMWM-ESP produced a metabolome heat map (Fig. 10B) that revealed distinct chemotypes and abundances of metabolites in the two crude extracts. Asparagine, urea, histidine, oxalic acids, fumaric acid, ornithine, ribose, glycemic acid, trehalose, lysine, valine, serine, isoleucine, and proline were abundant in LMWM-SE, whereas pyroglutamic acid, *trans*-4-hydroxyproline, phosphoenolpyruvate, succinic acid, gluconic acid, tartaric acid, glycerol, *meso*-erythritol, maltose, malic acid, alanine, lactic acid, and 3-phosphoglyceric acid were abundant in the LMWM-ESP (Fig. 10B).

GC-MS-based targeted identification of nonpolar metabolomes from LMWM-SE and LMWM-ESP. From the nonpolar fraction of LMWM-SE and LMWM-ESP of *A. caninum*, we identified 22 fatty acids (Table S2) comprising 17 saturated fatty acids, including stearic acid ($C_{18:0}$), palmitic acid ($C_{16:0}$), arachidic acid ($C_{20:0}$), margaric acid ($C_{17:0}$), and myristic acid ($C_{14:0}$), and 5 monounsaturated fatty acids, including elaidic acid ($C_{18:1}$), oleic acid ($C_{18:1}$), erucic acid ($C_{22:1}$), petroselinic acid ($C_{18:1}$), and nervonic acid ($C_{24:1}$). The nonpolar fraction of LMWM-ESP contained 13 fatty acids, with stearic acid ($C_{18:0}$), palmitic acid ($C_{16:0}$),

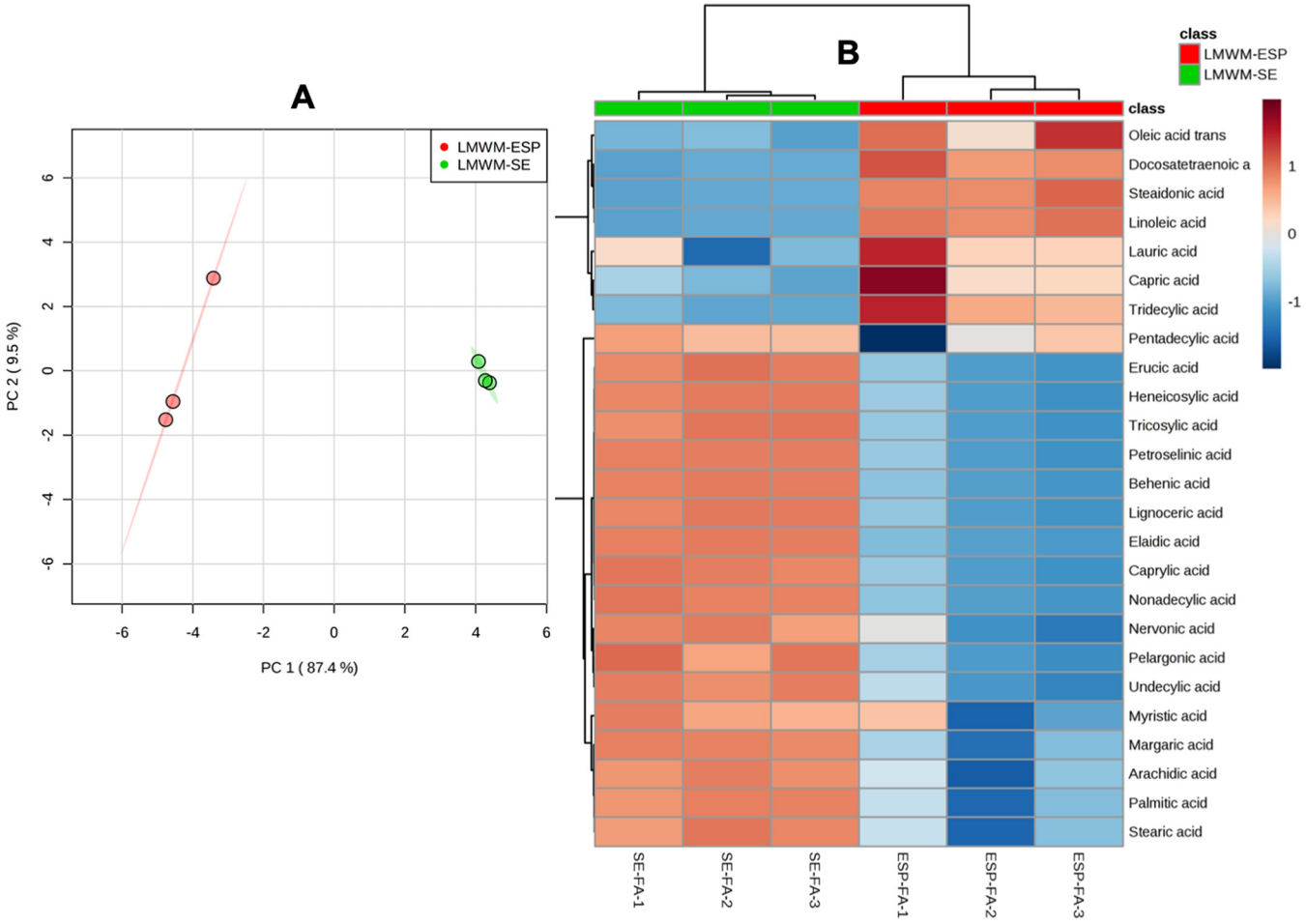

FIG 11 Multivariate analysis of sample groups containing nonpolar metabolites (lipids) of *A. caninum*. (A) PCA score plot showing clear separation of two groups, LMWM-SE and LMWM-ESP. (B) Heat map showing unsupervised hierarchical clustering of fatty acids present in LMWM-SE (SE-FA, somatic extract fatty acids) and LMWM-ESP (ESP-FA, excretory-secretory products fatty acids) ($n = 3$ biological replicates; distance measured using Euclidean metric and clustering using ward.D algorithm). Data analyzed by MetaboAnalyst 4 (samples normalized by median, log transformation, and autoscaling).

undecylic acid ($C_{11:0}$), linoleic acid ($C_{18:2}$), and tridecylic acid ($C_{13:0}$) representing the five most abundant metabolites based on peak area (Table S2). While 12 fatty acids were unique to only LMWM-SE, only 3 metabolites were exclusively found in LMWM-ESP. These three metabolites, including stearidonic acid ($C_{18:4}$), linoleic acid ($C_{18:2}$), and docosatetraenoic acid ($C_{22:4}$), are all unsaturated fatty acids and could potentially be candidates for anti-inflammatory activity. Ten metabolites were common to both the hookworm samples.

Multivariate chemometric analysis of the nonpolar metabolites of LMWM-SE and LMWM-ESP displayed good separation in a PCA plot (Fig. 11A). Cluster analysis of these two samples displayed as a metabolite heat map (Fig. 11B) revealed clearly separated chemotypes, compositions, and variances in the abundance of metabolites present in the two crude extracts.

LC-MS targeted analysis of LMWM-SE and LMW-ESP reveals the presence of short-chain fatty acids. A total of seven SCFAs were detected in the LMWM-SE and LMWM-ESP fractions using targeted LC-MS. LMWM-SE contained five SCFAs, with isobutyrate ($C_{4:0}$) as the major constituent. Other major SCFAs included propionate ($C_{3:0}$) and 2-methylvalerate ($C_{5:0}$) (Table 1). From LMWM-ESP, we identified six SCFAs, with propionate assuming the largest total peak area, followed by isovalerate (3-MBA; $C_{5:0}$), 2-methylbutyrate ($C_{5:0}$), acetate ($C_{2:0}$), isobutyrate, and butyrate ($C_{4:0}$) (Table 1). While isovalerate and 2-methylbutyrate were abundantly represented in LMWM-ESP, these two SCFAs were absent in LMWM-SE. In contrast, butyrate and 2-methylvalerate,

TABLE 1 SCFAs detected by LC-MS in LMWM-SE and LMWM-ESP of adult *A. caninum*

SCFA	Retention time (min)	Avg peak area	
		LMWM-SE	LMWM-ESP
Propionate ($C_{3:0}$)[a]	4.55	112,069	704,959
Isovalerate ($C_{5:0}$)	5.32	0	384,292
2-Methylbutyrate ($C_{5:0}$)	4.71	0	278,248
Acetate ($C_{2:0}$)[a]	3.92	96,109	198,281
Isobutyrate ($C_{4:0}$)	4.79	137,056	165,140
Butyrate ($C_{4:0}$)[a]	5.31	4,551	0
2-Methylvalerate ($C_{5:0}$)	8.51	105,324	0

[a]Reported anti-inflammatory activities of metabolites found in the nonpolar somatic extracts of *A. caninum* (64).

which were absent in LMWM-ESP, were present in abundance in LMWM-SE. Three common SCFAs found in both extracts were propionate, acetate, and isobutyrate.

DISCUSSION

Parasitic helminths, such as hookworms, have evolved to establish chronic infections in the human gut while inducing minimal pathology when present in low numbers (17). Hookworms regulate the immune system of the host for their benefit and subsequently promote a state of immune tolerance. This regulated environment not only promotes longevity for the parasites but also reduces the likelihood of developing diseases that result from a dysregulated immune system (27). A significant number of experimental and clinical studies support the immunoregulatory proficiency of parasitic helminths against distinct immunopathologies, including allergies, IBD, and other autoimmune diseases (9, 16, 28–31). While iatrogenic infection with hookworms and other helminths shows promise for treating numerous inflammatory diseases in humans, the therapy presents many challenges, including patient apprehension, standardization of treatment, and regulatory hurdles (17, 32). In an effort to exploit the therapeutic potential of hookworms without the need to infect patients with live worms, we and others showed that hookworm ESP proteins (>10 kDa) have potent immunomodulatory properties and can protect mice against pathology in different inducible models of colitis (17, 19, 20, 23, 33) and asthma (22). Nonproteinaceous metabolites derived from helminths, however, have received far less attention in terms of their molecular characterization and their immunoregulatory properties. Indeed, we recently proposed that helminth LMWM warrant in-depth investigation as an untapped source of new drugs for treating inflammation (24). Here we provide a molecular characterization of hookworm LMWM and assess the efficacy of different LMWM extracts and fractions in preventing both the onset of inducible colitis in mice and inflammatory cytokine production by primary human leukocytes.

Considering the relative strengths and limitations of all the available animal models, we chose the TNBS colitis model, which represents an intestinal immune response to environmental triggers, to investigate the anti-inflammatory properties of hookworm LMWM extracts. The TNBS model induces a mixed Th1/Th2/Th17 response (8), facilitating its use in screening for drugs targeting a broad range of inflammatory pathways. The intestinal mucosa of TNBS-treated mice is characterized by rapid production of cytokines such as IFN-γ, TNF-α, IL-1β, IL-13, and IL-17A (30). These cytokines are particularly important because disruption of the colonic mucosal layer by ethanolated TNBS dysregulates intestinal goblet cell function and elicits inflammation that drives the production of the cytokines. The colon contains epithelial goblet cells which are instrumental in controlling intestinal immune homeostasis by producing a protective mucus layer. Therefore, any extracts/small molecules from intestinal worms that can promote retention of colonic mucus and inhibit inflammatory cytokine production have therapeutic potential. We showed that mice treated with *A. caninum* LMWM extracts (both somatic extracts and ESP) promoted retention of healthy gastrointestinal architecture after TNBS administration; this took the form of normal mucosal crypts, large

numbers of unaltered goblet cells, and normal lamina propria and colon wall architecture in comparison to those of untreated groups that received TNBS. The colon culture supernatants and homogenates of mice treated with LMWM-ESP showed reduced expression of TNBS-induced TNF-α, IL-1β, and IL-13. Surprisingly, despite inducing significant protection against all assessed clinical and pathological parameters of colitis, treatment of mice with SE-HDA and SE-MeOH fractions did not result in significantly reduced levels of inflammatory cytokines in colonic tissue. Nonetheless, addition of SE-HDA to human PBMC resulted in significant suppression of TNF-α, IL-1β, IL-6, and the chemokine MCP-1. Despite conferring robust protection against TNBS-induced colitis in mice, the SE-MeOH extract did not suppress the production of LPS-stimulated cytokines by human PBMC. This could be due to distinct mechanisms of action of the bioactive components in each of the two models, or it might also reflect the presence of different bioactive metabolites in the two fractions. SE-HDA-induced suppression of inflammatory cytokines and chemokines was dose dependent and particularly potent for IL-1β and MCP-1. MCP-1 and other chemotactic cytokines, such as IL-8, induce chemotaxis, leukocyte activation, and granule exocytosis, all of which increase chronic inflammation and intestinal tissue destruction in IBD (34).

As a first step toward identifying the components that might contribute to the anticolitic effects of LMWM-SE and LMWM-ESP, we undertook a metabolomic analysis of these fractions. Both fractions contained a number of polar metabolites that likely reflect overflow of central carbon metabolism, as well as some more specialized pathways (35–39). Palmitic acid and stearic acid were the most common saturated fatty acids, present in all the hookworm extracts tested. Palmitic acid is the primary fatty acid from which other longer fatty acids are synthesized. Linoleic acid is found mostly in plant glycosides and is used by animals in the biosynthesis of prostaglandins (via arachidonic acid) and cell membranes (40). SCFAs, including acetic, propionic, methylbutyric, *n*-valeric, and methylvaleric acids, were first reported from the cuticle, muscle, and reproductive system of a nematode, *Ascaris lumbricoides* (41). Our findings concur with previous reports (39) on the presence of SCFAs in the ES products of *A. caninum*, in which volatile fatty acids such as acetic, propionic, isobutyric, and branched-chain C_5 acids were detected (39). More recently, saturated fatty acids were reported from the eggs of *A. caninum* (42), but the authors did not report the presence of SCFAs. The importance of SCFAs in human metabolism and disease has become evident recently, particularly in terms of perturbations in the microbiota (43, 44). The available literature suggests that helminths produce SCFAs *de novo*. For example, D-glucose-^{14}C labeling studies using *A. caninum* have shown that glucose is metabolized to produce acetate, propionate, and CO_2, while the amino acids L-valine and L-leucine are the precursors of isobutyric acid and isovaleric acid, respectively (39). The importance of SCFAs as intermediates in the energy metabolism of intestinal parasites in a succinate decarboxylase-dependent manner, as well as uncoupled mitochondrial respiration, has been reported (45). A recent review (46) suggested that formation and excretion of acetate as a metabolic end product of energy metabolism occur in numerous protist and helminth parasites.

A literature review on each of the 51 polar metabolites identified in LMWM-SE and LMWM-ESP revealed 12 polar metabolites with previously reported anti-inflammatory activities (47–57). LMWM-SE contained 11 anti-inflammatory polar metabolites, and LMWM-ESP contained only 8 polar metabolites with anti-inflammatory properties (Table S1). Similarly, of the 32 identified fatty acids (including SCFAs), only 10 were previously reported to have anti-inflammatory activity, including 6 saturated fatty acids (caprylic acid, capric acid, lauric acid, palmitic acid, methyl palmitate, and stearic acid), 1 unsaturated fatty acid (linolenic acid), and 3 SCFAs (acetate, propionate, and butyrate) (58–64). Of these, the three SCFAs have been reported to be effective in preventing inflammation associated with IBD (64). A comparative *in vitro* study of acetate, propionate, and butyrate revealed that propionate and butyrate were equipotent, whereas acetate was less effective at suppressing secretion of inflammatory cytokines associated with IBD from human neutrophils and colon organ cultures (64). SCFAs are particularly

important for colon homeostasis (65). For example, butyrate nourishes the colonic mucosa, and butyrate administration confers beneficial effects against IBD (65, 66). Butyrate and propionate have also been implicated in the maintenance of host immune function by signaling to epithelial cells, maintaining regulatory T cell populations, and inhibiting macrophage activation (67, 68).

Parasitic helminths modulate intestinal inflammation via alteration of the composition of the host gut microbiota. Moreover, helminths possess their own gut microbiota, which can be distinct from the host microbiota surrounding the parasite (69, 70). SCFAs are key metabolites and energy sources for commensal bacteria at the gut interface. For example, it is known that the gut microbiome is a complex ecosystem with microbial syntrophy at the intestinal mucosal interface (68) and that SCFAs such as acetate, butyrate, and propionate are produced and utilized by bacteria and benefit host epithelial cells by producing molecules like vitamin B_{12} (67). This mechanism has been demonstrated both in rodent models (71) and in human studies in which iatrogenic hookworm infection resulted in increased bacterial species richness and elevated production of SCFAs (11, 72). It is possible that *A. caninum* may actively skew the microbiome toward an anti-inflammatory composition by enhancing tolerogenic immune cross talk through SCFA production. Chronic infection with *Heligmosomoides polygyrus* altered the intestinal habitat, resulting in increased SCFA production that was transferable via the microbiota alone and was sufficient to mediate protection against allergic asthma (71). The resulting anti-inflammatory cytokine secretion and regulatory T cell suppressor activity required G protein-coupled receptor 41 (GPR-41), further highlighting the essential role of SCFAs produced by commensal microbe communities shaped by the presence of helminth infections. In the absence of metabolic labeling studies with microbiota-depleted worms, it is not possible to unequivocally determine the source of SCFAs in hookworms, and further studies are needed to define the contribution of the commensal microbiota to SCFA synthesis in this complex relationship of three very distinct yet coevolved taxa.

In summary, this study demonstrates that metabolites sourced from LMWM-SE and LMWM-ESP of *A. caninum* are diverse in nature and possess anti-inflammatory properties that can suppress colitis in mice and inflammatory cytokine production by human leukocytes. Several of these metabolites have been previously shown to have anti-inflammatory properties in various target diseases, including IBD. While it is difficult to obtain large quantities of hookworm ESP, in the future, efforts will be invested in further isolating the anti-inflammatory LMWM bioactive compounds given that these molecules have specifically evolved to interact with mammalian host tissues and play important roles in regulating inflammation.

MATERIALS AND METHODS

Hookworm and ESP collection. *A. caninum* adult worms were collected with clockmaker tweezers from the small intestines of infected dogs and transferred to prewarmed culture media (2% Glutamax in phosphate-buffered saline [PBS], 5% antibiotic/antimycotic [AA]) in 50-ml Falcon tubes. Worms were thoroughly washed with 5× antimycotic/antibiotic solution to purge bacterial contaminants and were cultured (50 worms per dish) in a single-component Glutamax medium (2% Glutamax in PBS supplemented with 2× AA) for 2 h at 37°C in 5% CO_2 to allow regurgitation/defecation of the host blood meal and other material (including bacteria) that may have been acquired from the dog host gut. The medium was replaced and excretory-secretory products (ESP) were collected twice each day (morning at 09:00 and afternoon at 16:30). Dead worms were removed from the culture plates every time the worms were fed with fresh culture medium. The ESP produced by live worms were collected for 4 to 5 consecutive days. The live adult worms were then snap-frozen in liquid nitrogen until further use.

Preparation of hookworm somatic tissue and ESP small-molecule/LMWM extracts. Adult *A. caninum* worms were frozen with liquid nitrogen and made into powder using a mortar and pestle. To obtain LMWM-SE, the powder was first soaked in a solvent mixture of hexane-dichloromethane-acetonitrile (1:1:1 vol/vol, 6 ml/g; HDA) for 30 min and was filtered (Whatman 4; qualitative circles, 185 mm; England International Ltd.). The extraction of cell material on filter paper was repeated three times with the same solvent. The filtrates were combined, centrifuged at 1,831 × *g* (Rotina 420 R; Hettich Zentrifugen, Germany) for 20 min at 4°C and the supernatant slowly transferred to round-bottom flasks. The solvent was removed using a Rotary Evaporator (G5 Heidolf CVC 3000 Vacuubrand) to obtain the somatic tissue HDA fraction (SE-HDA). The solid residue was snap-frozen in liquid nitrogen, powdered, and extracted with dichloromethane (3×). The filtration, centrifugation, and drying processes were

repeated as described above to obtain the DCM fraction (SE-DCM). The remaining somatic tissue was snap-frozen again, powdered, and extracted with methanol to obtain the MeOH fraction (SE-MeOH). The remaining solid residue from this step was snap-frozen and soaked in 5% HCl (pH 1 to 2). The supernatant was freeze-dried using a Scanvac Cool Safe to obtain acidified aqueous extract (SE-Acidic). The solid tissues were finally soaked in basified (NH_4OH, pH 10 to 12) water, filtered, centrifuged at 1,831 $\times$ *g*, and freeze-dried to obtain alkaline aqueous extract (SE-Basic). The whole ESP collected from *A. caninum* was centrifuged at 1,831 $\times$ *g* for 20 min at 4°C to remove eggs and debris, and the supernatant was filtered using 10-kDa-cutoff Amicon ultracentrifugal filters (Merck Millipore, Ireland; 15 ml) to get rid of macromolecules (proteins) and obtain only the required LMWM-ESP (<10 kDa). The LMWM-ESP was freeze-dried and stored at −80°C until further use. Stock concentrations of these extracts (1 mg/ml) were prepared by dissolving 1 mg of each lyophilized extract in 20 μl of dimethyl sulfoxide (DMSO), followed by addition of 980 μl of PBS. From each stock concentration, 50 μl was transferred to a vial and added to 150 μl of fresh PBS to make a total injectable volume of 200 μl/mouse to assess their efficacy in the TNBS model of acute colitis.

Animal ethics and source and housing of mice. The James Cook University (JCU) animal ethics committee approved all experimental work involving animals (ethics approval number A2199 and A2190). Mice were raised in cages in the JCU animal facility in compliance with the *Australian Code of Practice for the Care and Use of Animals for Scientific Purposes*, 7th ed. (73), and the Queensland Animal Care and Protection Act 2001. Age-matched 5-week-old male BALB/c mice were sourced from the Animal Resources Centre (Perth, Australia), weighed, placed in cages (5 mice per cage), and allowed to settle into the study facility for 4 to 5 days prior to the start of the experiment. Animals were housed in a temperature-controlled (26°C) and humidity-controlled (40 to 70%) environment, exposed to a 12-h day/night cycle, and provided with irradiated mouse chow supplied by Specialty Feeds (Glen Forrest, Western Australia) and autoclaved tap water *ad libitum*.

Experimental design and induction of TNBS colitis. We followed the modified experimental design and TNBS induction protocols described by us earlier (26). Briefly, mice were divided into three different groups: naive mice, mice receiving TNBS only, and mice receiving TNBS plus sample treatment. The experiments were performed in duplicate (total $n = 10$ mice/group). The samples were filtered using 0.22-μm sterile filters prior to intraperitoneal (i.p.) administration to mice. Each mouse in the sample treatment groups received 50 μl of extract suspension/mouse by i.p. injection (day 1). The TNBS-only and naive groups were administered 200 μl of PBS-DMSO (1%). Twenty-four hours after sample administration (day 2), the mice were anaesthetized by i.p. injection of anesthetic solution containing 50 mg/kg of body weight of ketamine and 5 mg/kg of xylazine. TNBS was administered by intrarectal (i.r.) injection of 100 μl of TNBS (2.5 mg/mouse) mixed with 50% ethanol using a soft catheter (Insyte Autoguard Shielded IV catheter 20 gauge b inch 1 pink; Becton, Dickinson). Mice were kept inverted for 2 min to prevent leakage of TNBS and returned to their cages. Mice were monitored daily until euthanized at day 5.

Monitoring colitis progression by clinical scoring. Mice were clinically scored for weight loss, piloerection, mobility, fecal consistency, and fecal pellet counts for 3 days following administration of TNBS. Each individual mouse was placed in a clean cage/open plastic jar and observed for 10 min to score the clinical symptoms. The changes in clinical signs of disease were scored from 0 to 2, 0 being normal and 2 being diseased. A score of 0 was given when the mice gained weight, 1 when weight remained the same, and 2 upon losing weight. Mice with no piloerection were scored 0, those with mild piloerection over the neck as 1, and those with severe piloerection all over the body as 2. The mobility of a mouse was scored as 0 for normal, 1 for movement only after stimulation, and 2 for hunched posture with no movement around the cage, even after stimulation. For fecal consistency, normal feces were scored 0, mild diarrhea was scored 1, and severe diarrhea with blood or no feces was scored 2. After 10 min of isolation, the fecal pellets were counted (a higher number of pellets indicated that mice were normal or were recovering from chemical colitis).

Assessing intestinal pathology and macroscopic scoring. On day 5 post-TNBS administration, the mice were euthanized. Their colons (from cecum to rectum) were surgically removed, measured, and assessed for changes in macroscopic appearance and pathological parameters, including adhesions, bowel wall thickening, and edema (scoring matrices of 0 to 3; 0 = normal, 1 = mild, 2 = moderate, and 3 = severe). The colons from each group were lined up on a clean surgical drape paper towel, their lengths were measured, and then the colons were transferred to a petri dish in sterile Dulbecco's PBS (DPBS). The tissues were opened longitudinally, washed with DPBS, placed under a microscope (Olympus SZ61, 0.67–4.5×), observed for inflamed sections, and scored for ulceration (0 to 3).

Evaluating colon histological structure. The distal colon tissue sections (1 cm) that were harvested from mice were placed in 4% paraformaldehyde (1 ml) to fix tissue overnight at 4°C and then transferred to 70% ethanol for storage. Tissue was embedded in paraffin and sectioned longitudinally for histology at a thickness of 4 μm. Sections were stained with hematoxylin and eosin (H&E) and observed for histological changes by light microscopy, and histological photomicrographs (×200) were captured. Each histological photomicrograph was blinded and then scored for changes in overall colon morphology and epithelial integrity. The cross sections of the colon tissues were scored for inflammation, edema, hyperplasia, ulceration, and number of goblet cells using a scoring matrix (74). An AxioCam Imager M1 (MRC ZEISS) was used for scoring the colon histology cross sections.

Cytokine ELISA with colon tissues. Colon pieces (1 cm) were collected and placed in sterile 24-well tissue culture plates with 500 μl of complete medium (RPMI medium containing 10% fetal bovine serum, 1% penicillin-streptomycin, 0.1% β-mercaptoethanol, 1% HEPES buffer). Tissues were cultured for 24 h at 37°C (supplied with 5% CO_2), after which supernatants were collected and stored at −80°C until further analysis. Colon culture supernatants were thawed and levels of cytokines were quantified using a

sandwich enzyme-linked immunosorbent assay (ELISA) (Ready-SET-Go!; eBiosciences) following the manufacturer's instructions. Values for optical density at 490 nm (OD_{490}) were measured using a POLARstar Omega plate reader (BMG LABTECH) and were expressed as picograms of tissue weight per milliliter.

Human PBMC collection and culture conditions. The human blood used for this project was donated by healthy volunteers. Written informed consent was obtained from each donor at the time of blood draw. Ethics approval for this research was obtained from the JCU Human Research Ethics Committee (approval number H7010). PBMC were isolated from whole blood by density gradient centrifugation using Ficoll-Paque media. For induction of T cell cytokines, PBMC were activated with a cell stimulation cocktail of 50 ng/ml of phorbol 12- myristate 13-acetate and 1 μg/ml of ionomycin (eBioscience) (PMA). PMA-stimulated cells were treated with 20 μg/ml of hookworm extracts (SE-HDA, SE-DCM, and SE-MeOH) or remained untreated. Due to the difficulty in obtaining sufficient quantities of *A. caninum* worms, we did not have enough LMWM-ESP to test with human cells. For stimulation of myeloid-associated cytokines, PBMC were activated with 10 ng/ml of lipopolysaccharide (LPS) (Sigma-Aldrich). LPS-stimulated PBMC were treated with 2 to 50 μg/ml of hookworm extracts (SE-HDA, SE-DCM, and SE-MeOH) or remained untreated. The cell culture plates were incubated overnight at 37°C and 6.5% CO_2. After incubation, the samples were centrifuged at 1,500 $\times$ *g* for 5 min and the culture supernatants were collected for cytokine analysis.

BD cytometric bead array. IL-1β, IL-6, IL-12, TNF-α, and MCP-1 from PBMC culture supernatants were quantified using a cytometric bead array (CBA) (BD Biosciences). The CBA assays were performed according to the manufacturer's instruction and run using a five-laser Special Order LSRFortessa with a high throughput sampler (BD Biosciences). Cytokine concentrations (in picograms per milliliter) were calculated based on the sample mean fluorescence intensities (MFI) compared to the cytokine standard curves. BD FCAP Array software version 3.0 was used for data analysis. Graphs and statistical analysis were produced using GraphPad Prism version 7.02 (GraphPad Software Inc.).

Cryomill extraction of adult worm fractions for GC-MS and LC-MS metabolomics analysis. *A. caninum* LMWM-somatic and LMWM-ESP (10 to 20 mg) were snap-frozen in liquid nitrogen to arrest metabolic changes, placed in cryomill tubes, then suspended in 600 μl of extraction solution (methanol-water, 3:1 [vol/vol], containing internal standards [^{13}C,^{15}N]valine and [^{13}C]sorbitol). The sample was extracted using a Precellys 24 Cryolys unit (Bertin Technologies) at 6,800 rpm with 3 30-s pulses (45-s interval between pulses) and a temperature of less than −5 °C (prechilled with liquid nitrogen). The homogenate was transferred to a fresh microcentrifuge tube on ice and chilled chloroform (150 μl) was added. The solution (chloroform-methanol-water 1:3:1 [vol/vol] monophasic mixture) was vortexed vigorously chilled on ice for 10 min with regular mixing and then centrifuged for 5 min at 0°C. The supernatant was transferred to a fresh 1.5-ml microcentrifuge tube on ice, and Milli-Q water (300 μl) was added to each tube to obtain a biphasic partition of the solution (chloroform-methanol-water, 1:3:3 [vol/vol]). The sample was vortexed vigorously and then centrifuged at 0°C for a further 5 min. Both the upper aqueous phase (methanol-water) and lower phase (chloroform) were derivatized and analyzed for polar and nonpolar metabolites, respectively.

Derivatization and targeted polar metabolite analysis using GC-MS. The upper aqueous phase (methanol-water, ~900 μl) was transferred to a fresh tube, then aliquoted (50 μl) into a pulled point insert, and dried in an evaporator (Christ RVC 2-33 CD; John Morris Scientific Australia) at 30°C. A further 50 μl of the aqueous sample was added every 30 to 40 min until completely dry. Samples were dehydrated by adding 50 μl of anhydrous methanol and then derivatized by addition of 20 μl of methoxyamine (30 mg/ml in pyridine; Sigma-Aldrich/Merck) at 37°C for 30 min, and then 20 μl of *N*,*O*-bis(trimethylsilyl) trifluoroacetamide (BSTFA) plus 1% trimethylchlorosilane (TMCS) (Thermo Fisher Scientific) was added prior to incubation at 37°C for 30 min. The derivatized sample (1 μl) was analyzed using an Agilent 7890 GC-MS (5973 MSD) (75). Chromatographic separation was achieved using an Agilent VF-5 ms column (30 m by 0.25 mm by 0.25 μm). Conditions for the oven were set at 35°C, held for 2 min, then ramped at 25°C/min to 325°C, and held for 5 min. Helium was used as the carrier gas at a flow rate of 1 ml/min, with compounds being detected across the *m/z* range of 50 to 600 atomic mass units (amu). The metabolomics data were analyzed in a targeted approach using Agilent's Mass Hunter Quantitative Analysis software (v.7). Target ion peak areas for polar metabolites were extracted using the in-house Metabolomics Australia metabolite library and output as a data matrix in the required format (.csv) for further analysis.

Targeted fatty acid analysis using GC-MS. The organic phase of the extraction (after removing a small amount for the pooled biological quality control [PBQC] samples) were sealed into GC vials and transesterified to create fatty acid methyl esters. For this, samples were mixed with 5 μl of Methprep-II (Alltech) using a Gerstel MPS2 autosampler robot, incubated for 30 min at 37°C with slow shaking for mixing. Fatty acid analysis was performed on an Agilent 7890 gas chromatograph coupled to a triple quadrupole (QqQ) mass selective detector (Agilent Technologies, Australia). Samples (2 μl) were injected in split mode (10:1) into an inlet set at 250°C, and chromatographic separation was achieved on an SGE BPX70 column (60 m by 0.25 mm [inside diameter] by 0.25-μm film thickness) (SGE, Australia). The oven conditions were 70°C for 1 min, then 40°C/min to 150°C, 4°C/min to 200°C, 3°C/min to 220°C, and 4°C/min to 250°C, with subsequent holding at 250°C for 4 min. Helium carrier gas flow was constant at 1.5 ml/min, and the MS transfer line was set at 280°C. Compounds were ionized using electron impact fragmentation (−70 eV), and mass spectra were collected in scan mode over the 50 to 450 *m/z* range at 3.6 scans/s.

Identification of SCFAs using LC-MS protocols. LMWM-somatic and LMWM-ESP were analyzed by LC-MS in accordance with previously described protocols (76). Samples were extracted using the same protocol as described above for cryomill extraction. A small portion (20 μl) of the extract was derivatized

using 3-nitrophenylhydrzine (3-NPH), which converted SCFAs to their 3-nitrophenylhydrazones. The samples (1 μl) were then injected into a Shimadzu LC 30AD-TQ 8060 triple quadruple mass spectrometer, using conditions similar to those previously described (76). Samples were analyzed in triplicate. Known SCFAs, including acetate, propionate, isobutyrate, butyrate, 2-methylbutyrate, isovalerate, valerate, 3-NPH, 2-methylvalerate, 3-methylvalerate, isocaproate, caproate, and heptanoic acid, were used as standards (5 μM and 50 μM concentrations).

Data analyses. The data from groups of mice from 2 independent experiments ($n = 10$) were combined and the statistical analyses were performed using GraphPad Prism (version 7.0) as described earlier (74). Comparisons were made between groups of treated mice administered with TNBS and untreated mice administered with TNBS; P values of < 0.05 were considered significant. When determining the differences between more than two groups with equal numbers of mice or samples but with more variables, 2-way analysis of variance (ANOVA) was used. For comparison of two or more groups with limited variables, a one-way ANOVA was applied. All results reported represent means $\pm$ standard errors of the means (SEM). The metabolomics data were analyzed in a targeted approach using Agilent's Mass Hunter Quantitative Analysis software (v.7). Target ion peak areas for polar and nonpolar metabolites were extracted using the in-house Metabolomics Australia metabolite library and were integrated and output as a data matrix for further analysis. Chemometric multivariate statistical analyses (PCA and heat map) were undertaken using MetaboAnalyst 4 (free online software [http://www.metaboanalyst.ca/]).

Literature searches of small molecules and their content analyses focusing on anti-inflammatory properties. Based on the list of small molecules identified from *A. caninum* extracts, we conducted a comprehensive literature survey for each compound. Surveyed literature mainly comprised the following databases: The Human Metabolome Database (HMDB), which contains 114,100 metabolite entries, including both water-soluble and lipid soluble metabolites (77); DrugBank, which contains information on 2,280 drug metabolites (78); and PubChem, which contains live record counts of 94,017,529 compounds (mostly small molecules) with data on chemical structures, identifiers, chemical and physical properties, biological activities, patents, health, safety, toxicity data, and many others (79). In addition, search engines, including Google Scholar and SciFinder Scholar, were used for tracing the references on biological activities of each compound. Unique search terms/keywords, including "biological activities," "anti-inflammatory," and "immune regulation," were used. Content analyses of these databases and references were performed focusing on the reported biological activities, and this information was then tabulated and cited against each compound.

SUPPLEMENTAL MATERIAL

Supplemental material for this article may be found at https://doi.org/10.1128/IAI.00851-18.

SUPPLEMENTAL FILE 1, PDF file, 0.2 MB.

SUPPLEMENTAL FILE 2, PDF file, 0.2 MB.

SUPPLEMENTAL FILE 3, PDF file, 0.1 MB.

SUPPLEMENTAL FILE 4, PDF file, 0.1 MB.

ACKNOWLEDGMENTS

This study was supported by an NHMRC Peter Doherty Early Career Researcher Fellowship (APP1091011) and AITHM Capacity Development Grant to P.W., an NHMRC program grant (APP1037304) and NHMRC Senior Principal Research Fellowship (APP1117504) to A.L., and an NHMRC Career Development Fellowship (APP1131732) to J.J.M.

We thank Makedonka Mitreva for hookworm genome analyses and Severine Navarro, Atik Susianto, Komal Kanojia, Vinod Narayana, and Bjoernar Hauge for assistance with cytokine analyses, SCFA method development for hookworm extracts, and animal husbandry.

REFERENCES

1. Crohn's & Colitis Foundation of America. 2014. The facts about inflammatory bowel diseases. Crohn's & Colitis Foundation of America, New York, NY.
2. Crohn's & Colitis Australia. 2014. Annual report 2012-2013. Crohn's & Colitis Australia, Camberwell, Australia.
3. Ng CS. 2016. Emerging trends of inflammatory bowel disease in Asia. Gastroenterol Hepatol (N Y) 12:193–196.
4. Jose FA, Heyman MB. 2008. Extraintestinal manifestations of inflammatory bowel disease. J Pediatr Gastroenterol Nutr 46:124–133. https://doi.org/10.1097/MPG.0b013e318093f4b0.
5. Hanlon I, Hewitt C, Bell K, Phillips A, Mikocka-Walus A. 2018. Systematic review with meta-analysis: online psychological interventions for mental and physical health outcomes in gastrointestinal disorders including irritable bowel syndrome and inflammatory bowel disease. Aliment Pharmacol Ther 48:244–259. https://doi.org/10.1111/apt.14840.
6. Niewiadomski O, Studd C, Hair C, Wilson J, Ding NS, Heerasing N, Ting A, McNeill J, Knight R, Santamaria J, Prewett E, Dabkowski P, Dowling D, Alexander S, Allen B, Popp B, Connell W, Desmond P, Bell S. 2015. Prospective population-based cohort of inflammatory bowel disease in the biologics era: disease course and predictors of severity. J Gastroenterol Hepatol 30:1346–1353. https://doi.org/10.1111/jgh.12967.
7. Brown C, Gibson PR, Hart A, Kaplan GG, Kachroo S, Ding Q, Hautamaki E, Fan T, Black CM, Hu X, Beusterien K. 2015. Long-term outcomes of colectomy surgery among patients with ulcerative colitis. Springerplus 4:573. https://doi.org/10.1186/s40064-015-1350-7.
8. Neurath MF. 2017. Current and emerging therapeutic targets for IBD. Nat

Rev Gastroenterol Hepatol 14:688. https://doi.org/10.1038/nrgastro.2017.138.
9. Croese J, Giacomin P, Navarro S, Clouston A, McCann L, Dougall A, Ferreira I, Susianto A, O'Rourke P, Howlett M, McCarthy J, Engwerda C, Jones D, Loukas A. 2015. Experimental hookworm infection and gluten microchallenge promote tolerance in celiac disease. J Allergy Clin Immunol 135:508–516. https://doi.org/10.1016/j.jaci.2014.07.022.
10. Gaze S, McSorley HJ, Daveson J, Jones D, Bethony JM, Oliveira LM, Speare R, McCarthy JS, Engwerda CR, Croese J, Loukas A. 2012. Characterising the mucosal and systemic immune responses to experimental human hookworm infection. PLoS Pathog 8:e1002520. https://doi.org/10.1371/journal.ppat.1002520.
11. Giacomin P, Zakrzewski M, Croese J, Su X, Sotillo J, McCann L, Navarro S, Mitreva M, Krause L, Loukas A, Cantacessi C. 2015. Experimental hookworm infection and escalating gluten challenges are associated with increased microbial richness in celiac subjects. Sci Rep 18:13797.
12. McSorley HJ, Gaze S, Daveson J, Jones D, Anderson RP, Clouston A, Ruyssers NE, Speare R, McCarthy JS, Engwerda CR, Croese J, Loukas A. 2011. Suppression of inflammatory immune responses in celiac disease by experimental hookworm infection. PLoS One 6:e24092. https://doi.org/10.1371/journal.pone.0024092.
13. Smallwood TB, Giacomin PR, Loukas A, Mulvenna JP, Clark RJ, Miles JJ. 2017. Helminth immunomodulation in autoimmune disease. Front Immunol 8:453. https://doi.org/10.3389/fimmu.2017.00453.
14. Blount J, Hooi D, Feary J, Venn A, Telford G, Brown A, Britton J, Pritchard D. 2009. Immunologic profiles of persons recruited for a randomized, placebo-controlled clinical trial of hookworm infection. Am J Trop Med Hyg 81:911–916. https://doi.org/10.4269/ajtmh.2009.09-0237.
15. Geiger SM, Fujiwara RT, Santiago H, Corrêa-Oliveira R, Bethony JM. 2008. Early stage-specific immune responses in primary experimental human hookworm infection. Microbes Infect 10:1524–1535. https://doi.org/10.1016/j.micinf.2008.09.003.
16. Croese J, O'neil J, Masson J, Cooke S, Melrose W, Pritchard D, Speare R. 2006. A proof of concept study establishing *Necator americanus* in Crohn's patients and reservoir donors. Gut 55:136–137. https://doi.org/10.1136/gut.2005.079129.
17. Loukas A, Hotez PJ, Diemert D, Yazdanbakhsh M, McCarthy JS, Correa-Oliveira R, Croese J, Bethony JM. 2016. Hookworm infection. Nat Rev Dis Primers 2:16088. https://doi.org/10.1038/nrdp.2016.88.
18. Yazdanbakhsh M, Kremsner PG, van Ree R. 2002. Allergy, parasites, and the hygiene hypothesis. Science 296:490–494. https://doi.org/10.1126/science.296.5567.490.
19. Ruyssers NE, De Winter BY, De Man JG, Loukas A, Pearson MS, Weinstock JV, Van den Bossche RM, Martinet W, Pelckmans PA, Moreels TG. 2009. Therapeutic potential of helminth soluble proteins in TNBS-induced colitis in mice. Inflamm Bowel Dis 15:491–500. https://doi.org/10.1002/ibd.20787.
20. Ferreira I, Smyth D, Gaze S, Aziz A, Giacomin P, Ruyssers N, Artis D, Laha T, Navarro S, Loukas A, McSorley HJ. 2013. Hookworm excretory/secretory products induce interleukin-4 (IL-4)+ IL-10+ CD4+ T cell responses and suppress pathology in a mouse model of colitis. Infect Immun 81:2104–2111. https://doi.org/10.1128/IAI.00563-12.
21. Mulvenna J, Hamilton B, Nagaraj SH, Smyth D, Loukas A, Gorman JJ. 2009. Proteomics analysis of the excretory/secretory component of the blood-feeding stage of the hookworm, *Ancylostoma caninum*. Mol Cell Proteomics 8:109–121. https://doi.org/10.1074/mcp.M800206-MCP200.
22. Navarro S, Pickering DA, Ferreira IB, Jones L, Ryan S, Troy S, Leech A, Hotez PJ, Zhan B, Laha T, Prentice R, Sparwasser T, Croese J, Engwerda CR, Upham JW, Julia V, Giacomin PR, Loukas A. 2016. Hookworm recombinant protein promotes regulatory T cell responses that suppress experimental asthma. Sci Transl Med 8:362ra143. https://doi.org/10.1126/scitranslmed.aaf8807.
23. Ferreira IB, Pickering DA, Troy S, Croese J, Loukas A, Navarro S. 2017. Suppression of inflammation and tissue damage by a hookworm recombinant protein in experimental colitis. Clin Transl Immunology 6:e157. https://doi.org/10.1038/cti.2017.42.
24. Shepherd C, Navarro S, Wangchuk P, Wilson D, Daly NL, Loukas A. 2015. Identifying the immunomodulatory components of helminths. Parasite Immunol 37:293–303. https://doi.org/10.1111/pim.12192.
25. Kaplan F, Srinivasan J, Mahanti P, Ajredini R, Durak O, Nimalendran R, Sternberg PW, Teal PE, Schroeder FC, Edison AS, Alborn HT. 2011. Ascaroside expression in *Caenorhabditis elegans* is strongly dependent on diet and developmental stage. PLoS One 6:e17804. https://doi.org/10.1371/journal.pone.0017804.
26. Wangchuk P, Navarro S, Shepherd C, Keller PA, Pyne SG, Loukas A. 2015. Diterpenoid alkaloids of *Aconitum laciniatum* and mitigation of inflammation by 14-*O*-acetylneoline in a murine model of ulcerative colitis. Sci Rep 5:12845. https://doi.org/10.1038/srep12845.
27. Varyani F, Fleming JO, Maizels RM. 2017. Helminths in the gastrointestinal tract as modulators of immunity and pathology. Am J Physiol Gastrointest Liver Physiol 312:G537–G549. https://doi.org/10.1152/ajpgi.00024.2017.
28. Leung J, Hang L, Blum A, Setiawan T, Stoyanoff K, Weinstock J. 2012. *Heligmosomoides polygyrus* abrogates antigen-specific gut injury in a murine model of inflammatory bowel disease. Inflamm Bowel Dis 18:1447–1455. https://doi.org/10.1002/ibd.22858.
29. Reardon C, Sanchez A, Hogaboam CM, McKay DM. 2001. Tapeworm infection reduces epithelial ion transport abnormalities in murine dextran sulfate sodium-induced colitis. Infect Immun 69:4417–4423. https://doi.org/10.1128/IAI.69.7.4417-4423.2001.
30. Weinstock JV, Elliott DE. 2013. Translatability of helminth therapy in inflammatory bowel diseases. Int J Parasitol 43:245–251. https://doi.org/10.1016/j.ijpara.2012.10.016.
31. Yang X, Yang Y, Wang Y, Zhan B, Gu Y, Cheng Y, Zhu X. 2014. Excretory/secretory products from *Trichinella spiralis* adult worms ameliorate DSS-induced colitis in mice. PLoS One 9:e96454. https://doi.org/10.1371/journal.pone.0096454.
32. Maizels RM. 2016. Parasitic helminth infections and the control of human allergic and autoimmune disorders. Clin Microbiol Infect 22:481–486. https://doi.org/10.1016/j.cmi.2016.04.024.
33. Cançado GGL, Fiuza JA, de Paiva NCN, Lemos LDCD, Ricci ND, Gazzinelli-Guimarães PH, Martins VG, Bartholomeu DC, Negrão-Corrêa DA, Carneiro CM, Fujiwara RT. 2011. Hookworm products ameliorate dextran sodium sulfate-induced colitis in BALB/c mice. Inflamm Bowel Dis 17:2275–2286. https://doi.org/10.1002/ibd.21629.
34. MacDermott RP, Sanderson IR, Reinecker HC. 1998. The central role of chemokines (chemotactic cytokines) in the immunopathogenesis of ulcerative colitis and Crohn's disease. Inflamm Bowel Dis 4:54–67. https://doi.org/10.1097/00054725-199802000-00009.
35. Fernando MA, Wong HA. 1964. Metabolism of hookworms. II. Glucose metabolism and glycogen synthesis in adult female Ancylostoma caninum. Exp Parasitol 15:284–292. https://doi.org/10.1016/0014-4894(64)90024-4.
36. Warren LG, Karlsson EL. 1965. Biochemistry of the dog hookworm. I. Oxidative metabolism. Exp Parasitol 17:1–19. https://doi.org/10.1016/0014-4894(65)90002-0.
37. Warren LG. 1970. Biochemistry of the dog hookworm. III. Oxidative phosphorylation. Exp Parasitol 27:417–423. https://doi.org/10.1016/0014-4894(70)90047-0.
38. Gimenez ME, Gimenez A, Gaede K. 1967. Metabolic transformation of 14C-glucose into tissue proteins of *Ancylostoma caninum*. Exp Parasitol 21:215–223. https://doi.org/10.1016/0014-4894(67)90083-5.
39. Warren LG, Poole WJ. 1970. Biochemistry of the dog hookworm II. Nature and origin of the excreted fatty acids. Exp Parasitol 27:408–416. https://doi.org/10.1016/0014-4894(70)90046-9.
40. National Center for Biotechnology Information. 2018. Linoleic acid. PubChem Compound Database; CID=5280450, https://pubchem.ncbi.nlm.nih.gov/compound/5280450 (accessed Apr. 16, 2018).
41. Beames CGJ. 1965. Neutral lipids of *Ascaris lumbricoides* with special reference to the esterified fatty acids. Exp Parasitol 16:291–299. https://doi.org/10.1016/0014-4894(65)90050-0.
42. Gyawali P, Beale DJ, Ahmed W, Karpe AV, Magalhaes RJS, Morrison PD, Palombo EA. 2016. Determination of *Ancylostoma caninum* ova viability using metabolic profiling. Parasitol Res 115:3485–3492. https://doi.org/10.1007/s00436-016-5112-4.
43. Morrison DJ, Preston T. 2016. Formation of short chain fatty acids by the gut microbiota and their impact on human metabolism. Gut Microbes 7:189–200. https://doi.org/10.1080/19490976.2015.1134082.
44. den Besten G, van Eunen K, Groen AK, Venema K, Reijngoud D-J, Bakker BM. 2013. The role of short-chain fatty acids in the interplay between diet, gut microbiota, and host energy metabolism. J Lipid Res 54:2325–2340. https://doi.org/10.1194/jlr.R036012.
45. Saz HJ. 1981. Energy metabolisms of parasitic helminths: adaptations to parasitism. Annu Rev Physiol 43:323–341. https://doi.org/10.1146/annurev.ph.43.030181.001543.
46. Tielens AGM, van Grinsven KWA, Henze K, van Hellemond JJ, Martin W. 2010. Acetate formation in the energy metabolism of parasitic helminths

and protists. Int J Parasitol 40:387–397. https://doi.org/10.1016/j.ijpara.2009.12.006.
47. Szél E, Polyánka H, Szabó K, Hartmann P, Degovics D, Balázs B, Németh IB, Korponyai C, Csányi E, Kaszaki J, Dikstein S, Nagy K, Kemény L, Erős G. 2015. Anti-irritant and anti-inflammatory effects of glycerol and xylitol in sodium lauryl sulphate-induced acute irritation. J Eur Acad Dermatol Venereol 29:2333–2341. https://doi.org/10.1111/jdv.13225.
48. Saxena RN, Pendse VK, Khanna NK. 1984. Anti-inflammatory and analgesic properties of four amino-acids. Indian J Physiol Pharmacol 28:299–305.
49. Mine Y, Zhang H. 2015. Anti-inflammatory effects of poly-L-lysine in intestinal mucosal system mediated by calcium-sensing receptor activation. J Agric Food Chem 63:10437–10447. https://doi.org/10.1021/acs.jafc.5b03812.
50. Ueki M, Ueno M, Morishita J, Maekawa N. 2013. D-ribose ameliorates cisplatin-induced nephrotoxicity by inhibiting renal inflammation in mice. Tohoku J Exp Med 229:195–201. https://doi.org/10.1620/tjem.229.195.
51. Hasegawa S, Ichiyama T, Sonaka I, Ohsaki A, Okada S, Wakiguchi H, Kudo K, Kittaka S, Hara M, Furukawa S. 2012. Cysteine, histidine and glycine exhibit anti-inflammatory effects in human coronary arterial endothelial cells. Clin Exp Immunol 167:269–274. https://doi.org/10.1111/j.1365-2249.2011.04519.x.
52. Unnikrishnan MK, Rao MN. 1990. Antiinflammatory activity of methionine, methionine sulfoxide and methionine sulfone. Agents Actions 31:110–112. https://doi.org/10.1007/BF02003229.
53. Abdel-Salam OM, Youness ER, Mohammed NA, Morsy SM, Omara EA, Sleem AA. 2014. Citric acid effects on brain and liver oxidative stress in lipopolysaccharide-treated mice. J Med Food 17:588–598. https://doi.org/10.1089/jmf.2013.0065.
54. Zhong Z, Wheeler MD, Li X, Froh M, Schemmer P, Yin M, Bunzendaul H, Bradford B, Lemasters JJ. 2003. L-glycine: a novel antiinflammatory, immunomodulatory, and cytoprotective agent. Curr Opin Clin Nutr Metab Care 6:229–240. https://doi.org/10.1097/01.mco.0000058609.19236.a4.
55. Cavone L, Calosi L, Cinci L, Moroni F, Chiarugi A. 2012. Topical mannitol reduces inflammatory edema in a rat model of arthritis. Pharmacology 89:18–21. https://doi.org/10.1159/000335094.
56. Echigo R, Shimohata N, Karatsu K, Yano F, Kayasuga-Kariya Y, Fujisawa A, Ohto T, Kita Y, Nakamura M, Suzuki S, Mochizuki M, Shimizu T, Chung U, Sasaki N. 2012. Trehalose treatment suppresses inflammation, oxidative stress, and vasospasm induced by experimental subarachnoid hemorrhage. J Transl Med 10:80. https://doi.org/10.1186/1479-5876-10-80.
57. Cicko S, Grimm M, Ayata K, Beckert J, Meyer A, Hossfeld M, Zissel G, Idzko M, Müller T. 2015. Uridine supplementation exerts anti-inflammatory and anti-fibrotic effects in an animal model of pulmonary fibrosis. Respir Res 16:105. https://doi.org/10.1186/s12931-015-0264-9.
58. Hoshimoto A, Suzuki Y, Katsuno T, Nakajima H, Saito Y. 2002. Caprylic acid and medium-chain triglycerides inhibit IL-8 gene transcription in Caco-2 cells: comparison with the potent histone deacetylase inhibitor trichostatin A. Br J Pharmacol 136:280–286. https://doi.org/10.1038/sj.bjp.0704719.
59. Huang WC, Tsai TH, Chuang LT, Li YY, Zouboulis CC, Tsai PJ. 2014. Antibacterial and anti-inflammatory properties of capric acid against *Propionibacterium acnes*: a comparative study with lauric acid. J Dermatol Sci 73:232–240. https://doi.org/10.1016/j.jdermsci.2013.10.010.
60. Aparna V, Dileep KV, Mandal PK, Karthe P, Sadasivan C, Haridas M. 2012. Anti-inflammatory property of n-hexadecanoic acid: structural evidence and kinetic assessment. Chem Biol Drug Des 80:434–439. https://doi.org/10.1111/j.1747-0285.2012.01418.x.
61. El-Demerdash E. 2011. Anti-inflammatory and antifibrotic effects of methyl palmitate. Toxicol Appl Pharmacol 254:238–244. https://doi.org/10.1016/j.taap.2011.04.016.
62. Ahmad M, Baba WN, Gani A, Wani TA, Gani A, Masoodi FA. 2015. Effect of extraction time on antioxidants and bioactive volatile components of green tea (*Camellia sinensis*), using GC/MS. Cogent Food Agric 1:1106387.
63. Kim DH, Yoo TH, Lee SH, Kang HY, Nam BY, Kwak SJ, Kim JK, Park JT, Han SH, Kang SW. 2012. Gamma linolenic acid exerts anti-inflammatory and anti-fibrotic effects in diabetic nephropathy. Yonsei Med J 53:1165–1175. https://doi.org/10.3349/ymj.2012.53.6.1165.
64. Tedelind S, Westberg F, Kjerrulf M, Vidal A. 2007. Anti-inflammatory properties of the short-chain fatty acids acetate and propionate: a study with relevance to inflammatory bowel disease. World J Gastroenterol 13:2826–2832. https://doi.org/10.3748/wjg.v13.i20.2826.
65. Wong JM, de Souza R, Kendall CW, Emam A, Jenkins DJ. 2006. Colonic health: fermentation and short chain fatty acids. J Clin Gastroenterol 40:235–243. https://doi.org/10.1097/00004836-200603000-00015.
66. Vinolo MAR, Rodrigues HG, Nachbar RT, Curi R. 2011. Regulation of inflammation by short chain fatty acids. Nutrients 3:858–876. https://doi.org/10.3390/nu3100858.
67. Belzer C, Chia LW, Aalvink S, Chamlaqain B, Piironen V, Knol JC, de Vos WM. 2017. Microbial metabolic networks at the mucus layer lead to diet-independent butyrate and vitamin B_{12} production by intestinal symbionts. mBio 8:e00770-17. https://doi.org/10.1128/mBio.00770-17.
68. Smith PM, Howitt MR, Panikov N, Michaoud M, Gallini CA, Bohlooly YM, Glickman JN, Garrett WS. 2013. The microbial metabolites, short-chain fatty acids, regulate colonic Treg cell homeostasis. Science 341:596–573.
69. White EC, Houlden A, Bancroft AJ, Hayes KS, Goldrick M, Grencis RK, Roberts IS. 2018. Manipulation of host and parasite microbiotas: survival strategies during chronic nematode infection. Sci Adv 4:eaap7399. https://doi.org/10.1126/sciadv.aap7399.
70. Plieskatt JL, Deenonpoe R, Mulvenna JP, Krause L, Sripa B, Bethony JM, Brindley PJ. 2013. Infection with the carcinogenic liver fluke *Opisthorchis viverrini* modifies intestinal and biliary microbiome. FASEB J 27:4572–4584. https://doi.org/10.1096/fj.13-232751.
71. Zaiss MM, Rapin A, Lebon L, Dubey LK, Mosconi I, Sarter K, Piersigilli A, Menin L, Walker AW, Rougemont J, Paerewijck O, Geldhof P, McCoy KD, Macpherson AJ, Croese J, Giacomin PR, Loukas A, Junt T, Marsland BJ, Harris NL. 2015. The intestinal microbiota contributes to the ability of helminths to modulate allergic inflammation. Immunity 43:998–1010. https://doi.org/10.1016/j.immuni.2015.09.012.
72. Cantacessi C, Giacomin P, Croese J, Zakrzewski M, Sotillo J, McCann L, Nolan MJ, Mitreva M, Krause L, Loukas A. 2014. Impact of experimental hookworm infection on the human gut microbiota. J Infect Dis 210:1431–1434. https://doi.org/10.1093/infdis/jiu256.
73. Australian Research Council. 2007. Australian code of practice for the care and use of animals for scientific purposes, 7th ed. Australian Research Council, Canberra, Australia.
74. Shepherd C, Giacomin P, Miller C, Navarro S, Loukas A, Wangchuk P. 2018. A medicinal plant compound, capnoidine, prevents the onset of inflammation in a mouse model of colitis. J Ethnopharmacol 211:17–28. https://doi.org/10.1016/j.jep.2017.09.024.
75. Overgaard AJ, Weir JM, De Souza DP, Tull D, Haase C, Meikle PJ, Pociot F. 2016. Lipidomic and metabolomic characterization of a genetically modified mouse model of the early stages of human type 1 diabetes pathogenesis. Metabolomics 12:13. https://doi.org/10.1007/s11306-015-0889-1.
76. Han J, Lin K, Sequeira C, Borchers CH. 2015. An isotope-labeled chemical derivatization method for the quantitation of short-chain fatty acids in human feces by liquid chromatography–tandem mass spectrometry. Anal Chim Acta 854:86–94. https://doi.org/10.1016/j.aca.2014.11.015.
77. Wishart DS, Jewison T, Guo AC, Wilson M, Knox C, Liu Y, Djoumbou Y, Mandal R, Aziat F, Dong E, Bouatra S, Sinelnikov I, Arndt D, Xia J, Liu P, Yallou F, Bjorndahl T, Perez-Pineiro R, Eisner R, Allen F, Neveu V, Greiner R, Scalbert A. 2012. HMDB 3.0—The Human Metabolome Database in 2013. Nucleic Acids Res 41:D801–D807. https://doi.org/10.1093/nar/gks1065.
78. Wishart DS, Feunang YD, Guo AC, Lo EJ, Marcu A, Grant JR, Sajed T, Johnson D, Li C, Sayeeda Z, Assempour N, Iynkkaran I, Liu Y, Maciejewski A, Gale N, Wilson A, Chin L, Cummings R, Le D, Pon A, Knox C, Wilson M. 2018. DrugBank 5.0: a major update to the DrugBank database for 2018. Nucleic Acids Res 46:D1074–D1082. https://doi.org/10.1093/nar/gkx1037.
79. Kim S, Thiessen PA, Bolton EE, Chen J, Fu G, Gindulyte A, Han L, He J, He S, Shoemaker BA, Wang J, Yu B, Zhang J, Bryant SH. 2016. PubChem Substance and Compound databases. Nucleic Acids Res 44:D1202–D1213. https://doi.org/10.1093/nar/gkv951.